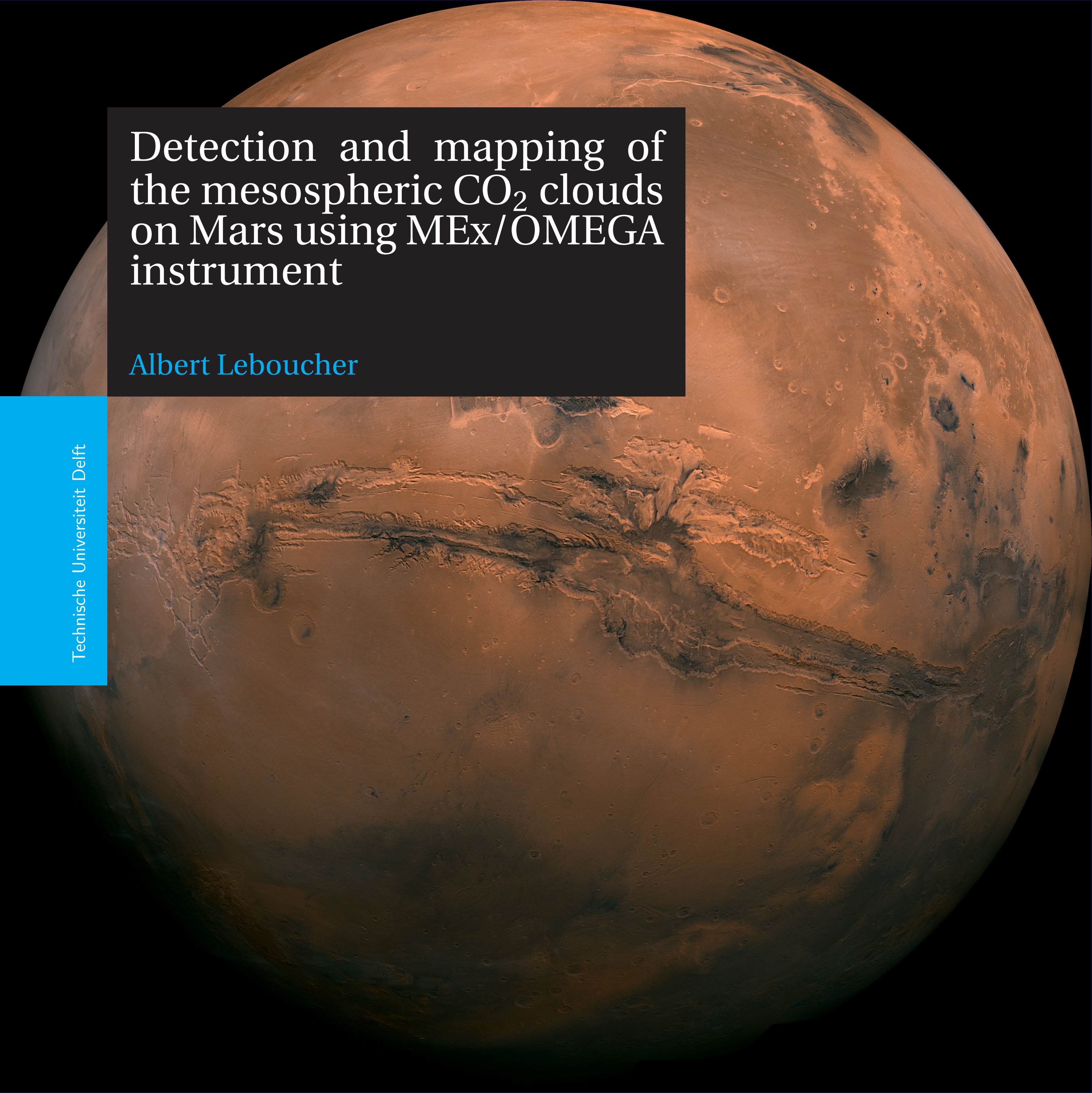

Detection and mapping of the mesospheric CO_2 clouds on Mars using MEx/OMEGA instrument

Albert Leboucher

Technische Universiteit Delft

TU Delft Delft University of Technology

Challenge the future

Detection and mapping of the mesospheric CO_2 clouds on Mars using MEx/OMEGA instrument

by

Albert Leboucher

in partial fulfillment of the requirements for the degree of

Master of Science
in Aerospace Engineering

at the Delft University of Technology,
to be defended publicly on Tuesday April 7, 2017 at 13:30 AM.

Student number:	4411994	
Project duration:	May 1, 2016 – February 15, 2017	
Supervisor abroad:	Dr. A. Määttänen	LATMOS, Guyancourt, France
Thesis committee:	Prof. Dr. Ir. P. Visser,	TU Delft, Chair of the commitee
	Dr. D. M. Stam,	TU Delft, Supervisor
	Dr. A. Menicucci,	TU Delft
	Dr. L. Rossi	TU Delft

Delft University of Technology

Special Thanks

First and foremost, I would like to thank my supervisor at LATMOS Anni Määttänen for managing me all along this period. Her experience and her advice helped me to move on during my Master Thesis through each obstacle and her happiness was a real source of motivation.

I also thank particularly Joachim Audouard, a post-doc with whom I worked a lot the past few months, for his good mood, his sincerity and his help when I needed some. He was always here to guide me and help me to understand the subtleties of my work.

Additionally, I would like to thank as well the whole team of doctoral students who welcomed me in the laboratory, showed me their work and what the research field looks like.

Finally, I would like to thank the Delft University of Technology for having taught me the required knowledge to the effective conduct of my Master Thesis, and particularly Daphne Stam, my supervisor there who always was available when I need her.

PREFACE

In 1997, the descent of the lander Pathfinder into the Martian atmosphere revealed temperatures in the mesosphere below CO_2 condensation point. As CO_2 is the main constituent of the martian atmosphere, the presence of mesospheric CO_2 ice clouds has been suggested, and then confirmed by spectro-imaging observations coming from satellite data. These clouds fascinate scientists because none of the current atmospheric models have been able to predict them. They also raise important questions about the martian mesosphere dynamics and properties. Since the early 2000s, a lot of instruments study these clouds in order to detect and map them. These observations are very important in order to be able to model better the atmospheric processes that take place on Mars as the CO_2 cycle has a significant impact on its climate. Several studies already developed methods to detect them but now these have to be improved and analysed better to fully characterise the clouds. What I am going to do will be then to analyse the three last years of observation from the OMEGA instrument onboard Mars Express, map the CO_2 clouds and study their distribution. The aim of this thesis will be to study the inter-annual variations and the properties of the clouds and try to correlate them with atmospheric parameters (amount of dust in the atmosphere, temperature, altitude) coming from other observations. The main objective here is to determine how these clouds form and what the source of the condensation nuclei is. With the results of our analysis, the climatology of Mars and its atmosphere dynamics will be refined.

Albert Leboucher
Delft, March 2017

Contents

List of Figures

1
INTRODUCTION

The atmosphere of Mars is mainly composed of CO_2 (about 95% of the atmospheric mass). Concerning the temperature, there is almost no greenhouse effect because the atmosphere is thinner than on Earth, and less solar flux arrives on the planet so it is colder with an average surface temperature of -55°C (218K). Early in the 1990s, the James Clerk Maxwell Telescope [1] recorded very low temperatures in the martian mesosphere close to the CO_2 condensation point at altitudes of 50-80km. From this point, scientists suggested that mesospheric clouds should form in this part of the atmosphere, thanks also to observations from Pathfinder [1] that revealed temperatures below CO_2 condensation point in this region. As CO_2 is the major constituent of the martian atmosphere and there is very little water vapour in the mesosphere, it was the most likely candidate to condensate. Several satellites have been then sent to study Mars (Mars Global Surveyor, Mars Express, Mars Odyssey...) helped by more and more sophisticated instruments (OMEGA, SPICAM, CRISM, MOC, TES, THEMIS), some of them used to characterise these clouds. They were observed in the equatorial mesosphere at the northern hemisphere summer and at northern and southern midlatitudes in autumn in the mid-2000s [2]. However, the observations did not allow analysis of their composition as they could be composed of water ice crystals or CO_2 ice crystals. In 2007, the presence of mesospheric CO_2 clouds was confirmed thanks to the OMEGA spectrometer revealing a CO_2 scattering peak around 4.24μm (see Section 5.1.1), within the CO_2 gaseous absorption band [3].

Several years of observations have then been published, listing and mapping all the mesospheric CO_2 clouds recorded (for instance, [4] and [5]). But these are raising important questions: How do these clouds form ? What is the source of the condensation nuclei ? What are their inter-annual variations ? What are their consequences for the martian atmosphere ? The main problem here, and what really intrigues scientists, is to explain the origin of these clouds. None of the current atmospheric models of martian atmosphere have indeed been able to predict them nor the observed temperatures. This is very important in order to understand the dynamics and properties of the martian atmosphere. Indeed, the CO_2 cycle has a great impact on Mars climate contributing to huge variations of the surface pressure over the year. Some studies developed methods to detect and map the clouds but there are still a lot of data that has not been analysed yet (about three martian years for instance for OMEGA). Moreover, the detection algorithms need to be improved to process the data more efficiently. The main objective is to do a climatology as complete as possible of these clouds.

I conducted my Master Thesis at LATMOS (Laboratoire, ATmosphères, Milieux, Observations Spatiales), which is a French space laboratory close to Paris. It is composed of several divisions according to the field of study (Planetary Sciences, the Earth, atmospheric layers...). The laboratory is engaged in a lot of projects by providing instruments for specific missions (SPICAM on MEx, SAM on Curiosity, Phebus on Bepicolombo...) and contributing to the science and publishing a lot of articles. LATMOS has also a lot of connections with other space laboratories that enables to have access to a lot of data coming from different instruments. Concerning Mars, LATMOS is at the front lines by having a team who studies the exobiology, chemistry and atmospheric processes of the planet.

This thesis has the following structure. In **Chapter 2**, the main characteristics of Mars are listed and compared to the Earth. One of the Mars Global Climate Models will be also described as well as the main hypotheses for cloud formation. In **Chapter 3**, a summary of the Martian cloud observations and studies that have been done over the past decades is given to understand better the current knowledge of the martian atmosphere and the different instruments used to characterise it. It will help us to put our study into the martian context. **Chapter 4** gives an overview of the Mars Express mission and describes all the instruments used for this study and the problems we faced, for example, to calibrate OMEGA. The **Chapter 5** explains the detection method used to map the CO_2 clouds on Mars and its improvements to avoid false detections. **Chapter 6** gives the main results of our study with our new list of CO_2 clouds found and their properties. Finally, **Chapter 7** discusses the condensation nuclei by bringing new insight and perspectives to fully conclude about their source.

2

MARS CHARACTERISTICS

In this chapter, general properties of Mars and its atmosphere will be given. Then, a brief summary of the Mars General Circulation Model (MGCM) is given, just to show how our results may help model the atmospheric processes that take place on Mars and explain their roles in the formation of mesospheric clouds and, inversely, how we can interpret our results thanks to the model. Finally, the main hypothesis concerning the source of the cloud condensation nuclei will be given.

2.1. GENERAL DESCRIPTION

This section aims at describing the general characteristics of Mars, which will help to understand how its atmosphere works. Mars is the fourth planet of the Solar System and formed about 4.5 billion years ago. Originally, the martian atmosphere is thought to have been denser, mostly composed of CO_2. However, it appears to have lost 99% of its mass 3.8 billion years ago due to the solar wind, probably caused by the absence of a strong magnetic field. Moreover, the gravity on Mars being three times lower than on Earth (3.7 m/s^2 vs 9.8 m/s^2), the planet cannot hold on to an atmosphere as dense as the Earth's. As a consequence, the martian atmosphere is very thin and principally composed of CO_2. The very low temperatures observed enable the formation of clouds in the atmosphere.

Mars is further away than the Earth from the Sun (1.5 AU vs 1 AU, where AU means "Astronomical Unit" and represents the average Earth-Sun distance). As a consequence, the solar flux at the top of the martian atmosphere is lower than on Earth (600 W/m^2 vs 1400 W/m^2). Finally, the surface pressure is about 100 times lower on Mars. This prevents the planet from having a large greenhouse effect, and causes huge temperature differences between day and night [6].

The atmosphere of Mars is composed of three distinct layers (see Figure 2.1):

- **Troposphere**: First atmospheric layer that extends to about 45 km. In this region, the temperature decreases almost adiabatically like in the troposphere on Earth because it is mostly heated through convection phenomena. Here it is the global circulation that dominates in the energy balance.
- **Mesosphere**: It goes from 45 km to 110 km. Mars does not have an equivalent of the terrestrial stratosphere (the layer between the troposphere and the mesosphere where the temperature increases with altitude, mainly due to the absorption of UV-flux by ozone) so the passage from the troposphere to the mesosphere is direct and induces a slowdown of the temperature decrease. Here it is the radiative effects that dominate the energy balance.
- **Thermosphere**: This part goes from 110 km to 200 km. Due to solar heating, the temperature increases as a function of the altitude. As the density is very small in this region, the gas molecules cannot get efficiently rid of their energy through collisions.

There are seasons on Mars as well. The obliquity of the planet is 25.2° (compared to 23.4° for the Earth) and its orbit is very eccentric (0.093 vs 0.017 for the Earth). As a consequence, the duration of the seasons and the associated heat received are different for both hemispheres. Due to these large variations, strong phenomena can occur like CO_2 condensation at both poles in winter (causing annual 20% atmospheric CO_2

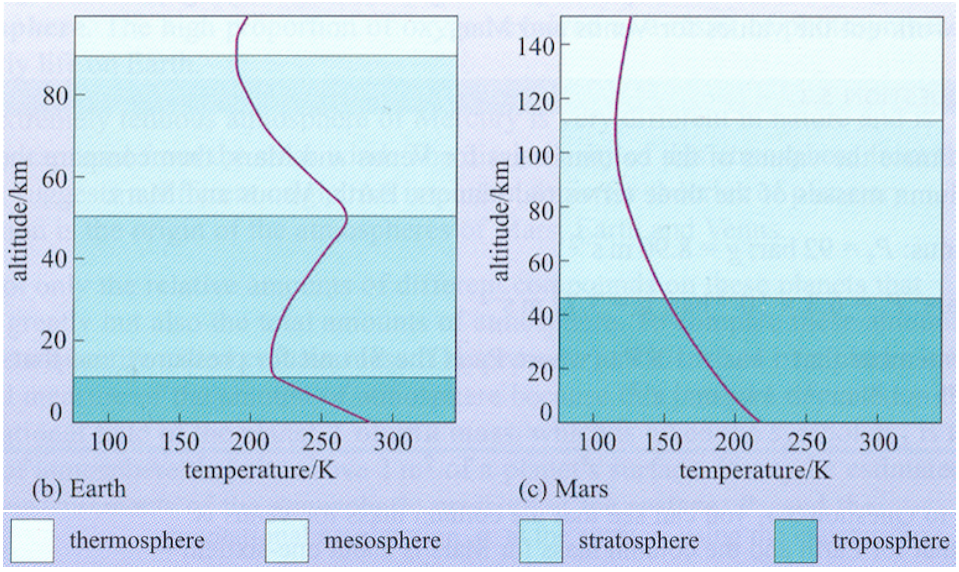

Figure 2.1: Comparison between the average temperature structure and atmospheric layers on Earth and on Mars (source: lasp.colorado.edu)

concentration variation as a large amount of CO^2 may be released during summer) or huge dust storms at the surface of the planet when it is close to its perihelion [7].

Finally, the atmosphere of Mars manifests dynamical phenomena such as gravity waves and, most essentially, thermal tides. There are indeed strong temperature variations between day and night. During daytime, dust absorbs solar radiation and re-emits it in the infrared heating the atmosphere and causing a huge increase in temperature, which then falls at night because of the thin atmosphere. These day-night temperature variations amplified by dust are the source of the formation and propagation of thermal tides in the Mars atmosphere. These tides define the coldest areas enabling CO_2 condensation (and so cloud formation) in the mesosphere [8]. They are the dominant effect in the thermal structure (see Chapter 7 for details).

There are multiple sources of aerosols on Mars. Principally, dust is lifted from the surface by the dust devils (at a very local scale) to regional or even global dust storms that may affect the entire planet. The dust particles serve as the condensation nuclei for some of the lower clouds in the martian atmosphere (less than 40 km altitude). There are indeed several types of clouds. First, there are water ice clouds, which form at lower altitudes thanks to higher formation temperatures, at both poles during winters and near the equator when L_s=20-160°. Then, there are of course the mesospheric CO_2 ice clouds that form at high altitudes (between 70 and 100 km) during northern spring, summer and autumn. They are less abundant and thinner than the previous ones. These clouds do not seem to really affect Mars climate as they have a very small radiative effect. In the past (billions of years ago), they may have had a bigger but limited impact [9]. Finally, CO_2 ice clouds also form at the poles during winter due to ice condensation at low altitudes (below 30 km). These are very important for the climate as they play a major role in the CO_2 cycle on Mars but they will not be discussed further. In the following, I will mainly focus on the mesospheric CO_2 ice clouds.

2.2. Description of the Mars General Circulation Model (MGCM)

In order to study and understand the dynamics of the atmosphere of a planet, it is necessary to implement a model based on the law of physics and validated with the current observations to reconstruct the atmospheric processes. This model has to take into account a lot of parameters, hypotheses and equations to simulate an atmosphere. By comparing then the model with the observations, one can conclude about its validity and how it can be improved. The aim of this section is then to detail the current model used by scientists from LATMOS and GCM (laboratory near Paris in France) to simulate the mesospheric clouds and determine how they form. In order to study atmospheric processes, models are needed to interpret the observations.

It is difficult to validate the modelled mesosphere as there are no large datasets for now. On the contrary, the lower atmosphere of Mars is well documented so it has been possible to validate this part. The mesospheric structure is thus an extension of it. The hypotheses and equations of the model can be found in [8].

Thanks to this, it is possible to obtain theoretical temperature profiles in the martian mesosphere. When these results are compared to the observations, it has been seen that the temperatures calculated by the model are not low enough to enable CO_2 condensation at the considered altitudes and locations (the temperatures are still 10-15K above the limit). However, the model predicts well the temperature minima at the altitude, location and season of the clouds. Likewise, the estimated wind speeds are mostly in agreement with the observations. As explained in section 2.1, thermal tides due to large temperature variations between daytime and nighttime define the coldest area in the martian mesosphere. The temperatures that the model predicts for the lower atmospheric regions are in accordance with the observations. However, the mesospheric temperatures found with the model are still too high to enable the formation of clouds in this part of the atmosphere (see Figure 2.2).

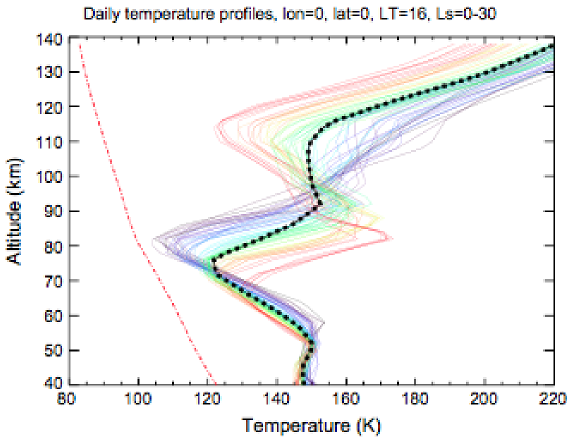

Figure 2.2: The individual daily temperature profiles from the MGCM temperatures at the equator and prime meridian for the first "month" of the Martian year Ls = 0-30° for the local time (LT 16) of the coldest temperatures at cloud altitudes. The black dashed line represents the monthly- averaged temperature. The red dash-dotted line is the condensation temperature of CO2 [5].

The reason why the model does not predict supersaturation of CO_2 may be because gravity waves propagating vertically are needed to locally perturb mesospheric structure and allow for temperatures below CO_2 condensation point [10]. These gravity waves are not modelled as they are small scale phenomena. Their propagation is well-known but the resolution of the atmospheric model (composed of grids that are about 200 km wide) is too low to enable their implementation. The temperatures computed by the MGCM are indeed 10-15K above this point, but a local perturbation might cause a drop of temperature favouring cloud formation, and gravity waves are able to cause that kind of phenomenon. This needs further study to fully conclude about the cloud formation conditions.

2.3. SOURCE OF CONDENSATION NUCLEI

In this section, we will discuss the current knowledge about the formation process of the mesospheric CO_2 ice clouds. More particularly, the different hypotheses concerning the nucleation will be given.

2.3.1. INTRODUCTION

As already explained, it might be the presence of gravity waves propagating vertically that perturb the mesosphere locally and allow for temperatures below CO_2 condensation point. Usually, a cloud forms thanks to condensation nuclei (dust, meteoritic smoke) and temperatures low enough to enable the condensation of an element (CO_2 or H_2O) around this nucleus to create cloud particles. But here are two aspects needing further explanations: what are the elements that could condense ? And, above all, what is the formation process ?

Concerning the first point, the local vapour supply has to be studied. CO_2 is the major constituent of the martian atmosphere so it is likely to condense in some parts of the mesosphere. The low temperatures recorded in the martian mesosphere (where the pressure is around 0.01Pa) might enable CO_2 molecules to condensate as shown in Figure 2.3. On the other hand, the instrument SPICAM has observed water vapour supersaturation at high altitudes and OMEGA observed one H_2O cloud in the mesosphere.

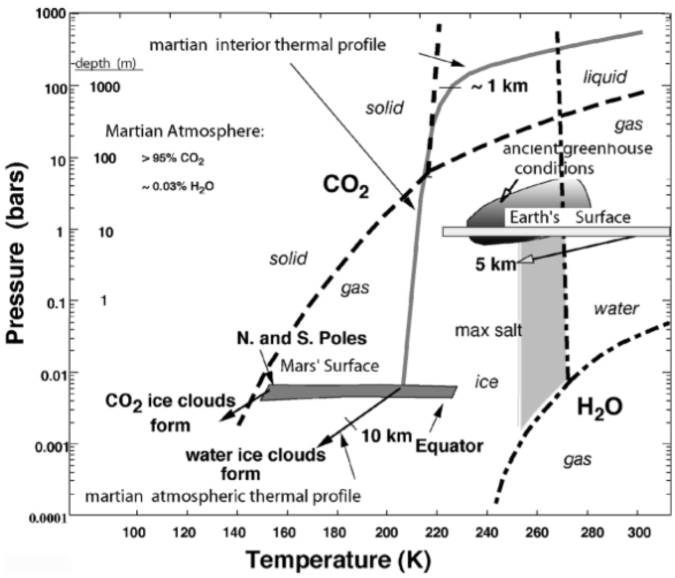

Figure 2.3: Pressure-temperature regimes from the interior of Mars to its atmosphere compared to the phase diagrams of CO_2 (dashed curve) and H_2O (dash-dotted curve) [11].

There is no mystery to explain the H_2O cloud formation. The formation conditions are easier than for CO_2 clouds as they form at higher temperatures. Besides, as they form at lower altitudes (around 40 km), the condensation nuclei are undoubtedly dust in the atmosphere. Models have even been able to reproduce their formation using this hypothesis and are in agreement with the observations.

There are several possible formation processes for the CO_2 ice clouds. These will be presented in the following.

2.3.2. TYPES OF NUCLEATION PATHWAY

The nucleation theory enables to understand the change of phase of CO_2 crystals: it describes the aggregation of ice molecules into the vapour phase and so the formation of cloud particles. The important point here is the source of the condensation nuclei. There are indeed two possible nucleation pathways: homogeneous and heterogeneous. The first one does not require any condensation nuclei but strongly supersatured cold pockets enabling the CO_2 to condense. The second one needs however a source of condensation nuclei to enable the growth of the CO_2 ice particle. Each formation theory will be described.

Homogenous nucleation

This nucleation process is the most elementary as it does not require any source of condensation nuclei. The CO_2 molecules aggregate with each others to form cloud particles. However, it needs to reach a certain amount of energy to enable this formation. The saturation ratio is a crucial variable to understand this phenomenon.

$$S = \frac{p_v}{p_{sat}(T)} = \frac{x_v * p}{p_{sat}(T)}$$

where p is the atmospheric pressure, p_v is the partial pressure of CO_2 in the atmosphere (about 95% of the total pressure) and $p_{sat}(T)$ the saturated vapour pressure.

This ratio depends on the temperature T and enables to assess the amount of molecules in vapour phase compared to the amount of molecules in thermodynamic equilibrium. If S>1, the atmosphere is said to be "supersatured". As a consequence, at a certain pressure level (or altitude), the saturation ratio will increase only if the amount of CO_2 molecules is larger or if the temperature is smaller (as p_{sat}(T) decreases exponentially with decreasing temperature).

Figure 2.4 shows the variation of the saturation ratio of CO_2 molecules as a function of the difference between the condensation temperature T_{cond} and the temperature T for two values of pressure (at the surface and at 80-90km)

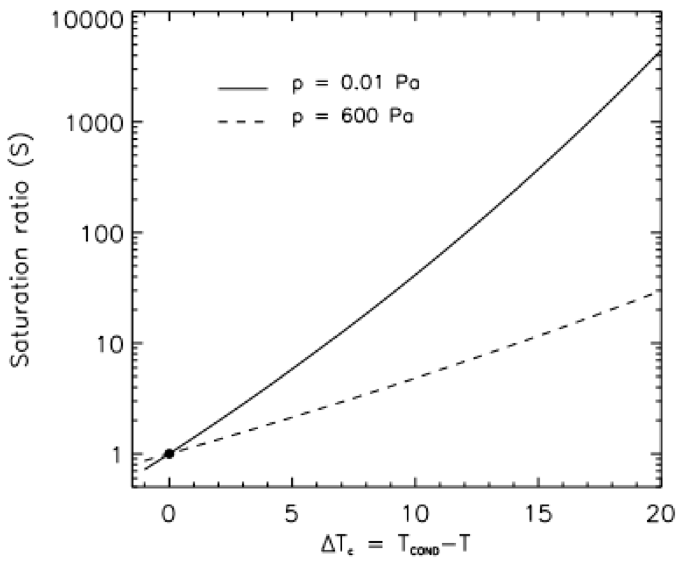

Figure 2.4: Saturation ratio of CO_2 as a function of the difference between the condensation temperature T_{cond} and the temperature T for two values of pressure: P=600Pa at the surface and P=0.01Pa at 80-90km [7].

However, the condition S>1 is not sufficient to enable phase changing. It needs to reach a critical value S_c in order to get enough energy. In other words, the atmospheric temperature has to be lower than the required condensation temperature, that is to say, it needs then to be very low in this case. Thus, very high supersatured cold pockets are required to enable homogeneous cloud formation. Actually, such supersatured pockets have been observed with SPICAM even if these pockets were located above the clouds (details on this instrument can be found in Section 4.4) [2]. As a consequence, homogeneous nucleation may happen if the saturation ratio is large enough.

Calculations made in [5] shows that homogenous nucleation in the mesosphere (around 80-90km altitude) needs really intense conditions in terms of saturation ratios ($S_{sat}\approx 10^{15}$) and temperature deviations ($\Delta T\approx$50K). Thus, it means that the mesospheric temperatures have to be around 50K (as $T_{cond}\approx$100K) to allow for homogeneous nucleation and such values have never been observed until now. This is why the heterogeneous nucleation hypothesis is preferred, which will be described in the next section.

Heterogeneous nucleation

The principle of heterogeneous nucleation has the same basis as homogeneous nucleation but it uses a source of condensation nuclei (aerosol, dust, meteoritic smoke...) to decrease the required energy level (and so the saturation ratio) for particles formation. This process is mostly responsible for cloud formation on Earth and, perhaps, Mars. The full analytical study of this phenomenon can be found in [7] and will not be detailed here.

Assuming a nuclei size of 1nm, the saturation ratio and the associated temperature deviation is much lower than for homogeneous nucleation ($S_{sat}\approx$300 and $\Delta T\approx$15K) [5]. It is consistent with the observed temperatures found with SPICAM [2]. It shows that heterogenous nucleation is the most likely process that explains CO_2 cloud formation on Mars.

Nevertheless, there are still questions about the condensation nuclei for the CO_2 clouds because of observational biases with OMEGA (insufficient coverage for the Martian Years 27, 28 and 29). Dust particles are unlikely candidates because even if storms eject dust into Mars mesosphere, it would not stay long enough at high altitudes to enable the formation of such clouds. Assuming a large dust storm brings a lot of particles in the martian mesosphere, simulations have been implemented to calculate how long they could stay before falling out ([12], [13]). They show that the dust particles did not stay high long enough to explain the cloud formation periods. In addition, dust storms usually happen only near the perihelion of Mars, that is to say for L_s=220-300°, long before the cloud formation starts. As a consequence, the most probable hypothesis for the condensation nuclei are meteoritic smoke particles as there is a constant meteoritic particle layer in the martian mesosphere. These particles have also been observed on Earth and might be the source of the condensation nuclei for the terrestrial mesospheric clouds (also called noctilucent clouds) that form between 80 and 90 km and that are composed of water ice particles.

3

OBSERVATIONS

Mars has always been a source of fantasy for mankind. The first observations of the planet from space were done in the 1970s by the spacecrafts Mariner 6 and 7. They were the first spacecrafts to detect emission peaks in the CO_2 ice band region (around 4.3 μm) but at low altitudes (around 20 to 30 km). The hypothesis of the presence of mesospheric clouds on Mars was made since quite a while but it is only in 1997, thanks to the descent of the lander Pathfinder into Mars atmosphere, that temperatures below CO_2 condensation point were effectively observed [1] at higher altitudes. Besides, Pathfinder made ground-based observations and observed blue high altitude clouds from the surface before sunrise (see Figure 3.1).

Figure 3.1: Photos of clouds on Mars taken during nighttime by Pathfinder (on the left) and during daytime by Sojourner (on the right). Source: NASA/JPL.

From this point, even if there was no real evidence about their composition, it was supposed that CO_2 ice clouds exist on Mars. Since, with the help of further missions (Mars Global Surveyor, Mars Express, Mars Odyssey), mesospheric clouds were undoubtedly detected during northern spring and summer at the equator and during northern autumn at northern and southern mid-latitudes. It was thought that most of the mesospheric clouds were composed of CO_2 ice as it is the major constituent of the martian atmosphere [9]. Moreover, carbon dioxide supersaturated pockets were observed close to the clouds [2], giving further evidence to the presence of CO_2 mesospheric clouds on Mars.

Several studies have been published on this topic (for instance, [2], [3], [4], [14]), which confirm that the high-altitude clouds were composed of CO_2 (the spectrometers revealed a scattering peak at 4.24 μm that could be related to CO_2 ice crystals at high altitude). Since then, many articles used the data coming from the instruments (imagers, spectrometers) in orbit around Mars to map and describe the distribution of the clouds in the atmosphere as well as their internal structure ([5], [15]). H_2O clouds were of course also observed but at lower altitudes (around 40 km and only one at 70 km). Besides, by using instruments simultaneously (see Chapter 4), some of the clouds were observed with high spatial resolution, presenting the first context images of this phenomenon and enabling to determine their altitudes and speeds. It is then possible to make the difference between a CO_2 and a H_2O cloud by looking at their absorption peaks and altitude. Some studies using other instruments and a radiative transfer model of the martian atmosphere also concluded that the mesospheric equatorial clouds were mostly composed of CO_2 [16].

In total, there are about 9 Martian Years (MY) of mesospheric cloud observations coming from Mars Express but with a limited coverage as most of the data come from nadir observations (very few observations at the limb to study the vertical distribution of atmospheric components). Moreover, the temporal resolution is too variable according the years to draw conclusions. All these data and studies are very important in order to be able to construct a climatology of martian clouds as complete as possible. By doing this, it will be possible to describe further and maybe conclude about the mesospheric structure and dynamics of Mars, as very specific conditions (especially low temperatures and pressure) are required to enable for CO_2 ice condensation. These CO_2 ice clouds are very important due to the impact of the CO_2 cycle on Mars climate, even of their contribution into it should be relatively low as they are very thin. As the amount of CO_2 gas in the atmosphere varies a lot over the year, the surface pressure on Mars changes too (see Figure 6.3).

4

Description of the instruments used

In this chapter, an overview of the Mars Express mission will be given firstly. Then, the main instruments used during my thesis to map and characterise the mesospheric CO_2 clouds will be described.

4.1. Overview of Mars Express

In this section, the Mars Express mission will be described further such as its orbit and its main scientific objectives as well as all the instruments on-board. It will help to understand why it is the OMEGA instrument that is used for our study rather than the others.

4.1.1. General description of Mars Express

Mars Express (see Figure 4.1) is a probe conceived by the European Space Agency (ESA) and launched in 2004 (still operating now). It is so called because of its low cost and development time. Indeed, several instruments on-board this probe were originally designed for the Russian Mars mission in 1996. However, the launcher (and so the satellite) exploded during its launch. As a consequence, ESA with help of industries and scientists decided to send a new satellite using pre-made instruments. This enables to significantly reduce the development time and costs needed for such a mission. Indeed, the development time was only 6 years and its cost around 150 M€.

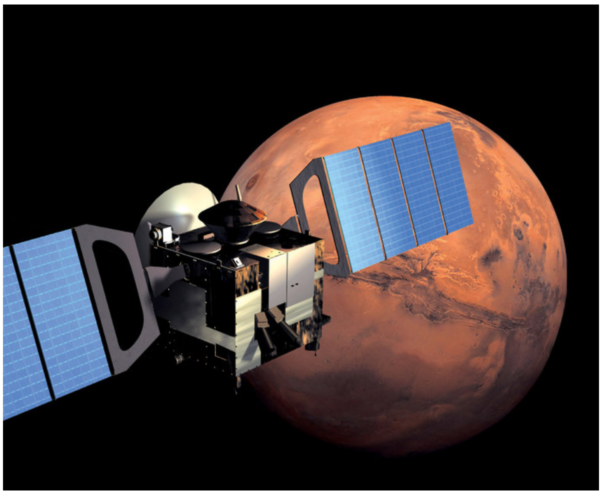

Figure 4.1: The Mars Express probe orbiting Mars (Credit: ESA).

Objectives The main objectives of the mission are to study the whole planet from its geology and minerals to its atmosphere and climate. Another goal is to look for water traces below the surface the planet and so conclude if the environmental conditions in the past on Mars were suitable for life.

Results As already mentioned, the Mars Express probe was launched in 2003 and it is still operating. Thanks to these 12 years of data, the main goals of the mission have been reached:

- Mars has been almost totally mapped (as well as its moons Phobos and Demos) and some phenomena such as dust storms and clouds were perfectly observed
- Some hydrated minerals, water ice beneath the surface and complex structure that could only form with the presence of water were discovered. The mission has also enabled to demonstrate that the past environmental conditions were suitable for life.
- The probe has also a given a detailed description of martian atmosphere with the proportion of all its chemical components, highlighting the possible presence of methane.
- It has also helped to relay information between the rovers (from NASA) at the surface and the Earth

As a consequence, Mars Express is considered as a successful mission thanks to all its achievements.

Orbit of Mars Express The Mars Express probe was launched the 2nd of June, 2003 and entered in orbit around Mars the 25th of December, 2003. It can be noted that a lander Beagle 2 was also present on-board the satellite and it was released the 19th of December into Martian atmosphere but no signal was received since its entry. As a consequence, it was declared unsuable.

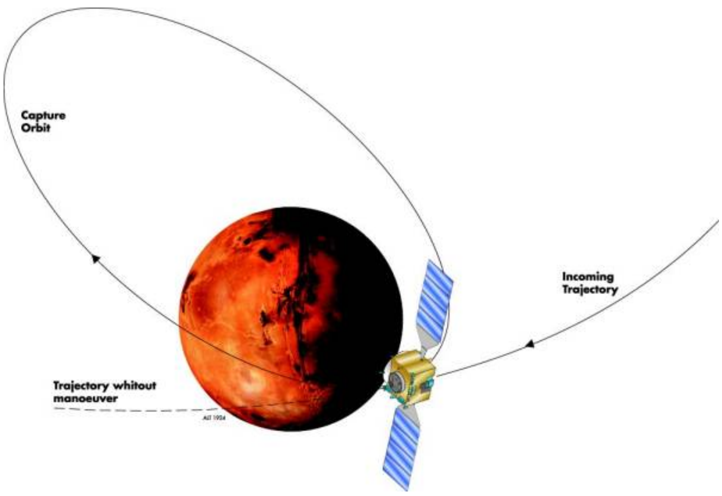

Figure 4.2: Orbit insertion of the Mars Express probe (Credit: CNES).

The probe was inserted into an elliptical orbit with an aphelion of 298km and a perihelion of about 10142km (see Figure 4.2). Its orbit is also near-polar with an inclination of 86°.

4.1.2. INSTRUMENTS ON-BOARD

In this section, we will discuss the instruments on-board Mars Express and their scientific objectives. Mars Express hosts seven instruments: three aim at studying the surface and the subsurface of Mars, three others the atmosphere and the last one the gravitational field of Mars. They are listed below:

- **OMEGA** (Observatoire pour la Minéralogie, l'Eau, les Glaces et l'Activité): it is a visible and infrared spectrometer that primary enables to map the minerals at the surface but also thanks to its large wavelength range, it is able to study the clouds that form in the atmosphere. The PI (Principal Investigator) of OMEGA is Jean-Pierre Bibring from the Institut d'Astrophysique Spatiale (IAS) in Orsay, France. This instrument is particularly interesting for our study and will be described further in Section 4.2.
- **HRSC** (High-Resolution Stereo Camera): it is an imager that is able to take high-resolved pictures of the surface (about 10 metres resolution) and so study very precisely the topography of Mars. The PI is Gerhard Neukum from Freie Universität in Berlin, Germany. This instrument will be detailed in Section 4.3.

- **MARSIS** (Mars Advanced Radar for Subsurface and Ionosphere Sounding): this instrument sounds and maps the subsurface of Mars (few kilometres depth) by using low frequency radio. It will help to reveal the presence of water ice beneath the surface. The PI of this instrument is Giovanni Picardi from Universita di Roma 'La Sapienza' in Rome, Italy.

- **PFS** (Planetary Fourier Spectrometer): it is able to derive the temperature and pressure profile of CO_2 through the atmosphere and look for trace gases. The PI of this instrument is Vittorio Formisano from Istituto Fisica Spazio Interplanetario in Rome, Italy.

- **SPICAM** (SPectroscopy for the Investigation of the Characteristics of the Atmosphere of Mars): it measures the concentration of ozone and water vapour over the whole planet for each season. It will be discussed further in Section 4.4. The PI is Jean-Loup Bertaux from LATMOS in Guyancourt, France.

- **ASPERA** (Analyser of Space Plasmas & EneRgetic Atoms): it aims at studying the interactions between the upper atmosphere of Mars and the solar wind and so the loss of atmosphere as there is no longer magnetic field on Mars. The PI is Rickard Lundin from the Swedish Institute of Space Physics in Kiruna, Sweden.

- **MaRS** (Mars Radio Science Experiment): it uses subsystem that relays information and data between the spacecraft and the Earth in order to study the variation in the gravitational field of Mars and the surface roughness. The PI of this instrument is Martin Pätzold from Köln University in Germany.

By describing each instrument on-board the Mars Express probe, we now know their role and scientific mission and we understand better why it is OMEGA that is preferred for our study. This instrument and its characteristics are described further in the following section.

4.2. OMEGA

4.2.1. DESCRIPTION

Definition

As already mentioned, OMEGA is an imaging spectrometer conceived at IAS and developed in collaboration with Italy [17]. Originally, it was realised for the Russian mission Mars 1996, which failed. This instrument functions in several wavelength ranges: the visible and the near-infrared (see Figure 4.3). As explained in [5], the spectral range of this instrument is between 0.38 μm and 5.1 μm in 352 spectral elements (called in the following 'spectel'). It is composed of two channels: one for the visible and the other for the infrared, the latter in addition divided into two parts according to the short or long wavelengths:

- The visible channel is composed of 96 spectels between 0.35 μm and 1.07 μm

- The short-infrared, referred as "C-channel", is composed of 128 spectels between 0.93 μm and 2.73 μm

- The long-infrared, referred as "L-channel" and used to detect the clouds, is composed of 128 spectels between 2.53 μm and 5.1 μm

As the CO_2 ice absorption band is around 4.3 μm, the channel recording the long-infrared is mostly used for CO_2 cloud characterisation. The OMEGA observations consist of datacubes, one for each observational session (these sessions are named with the convention #orbit_session, for instance #551_3). These cubes are 3-dimensional objects with the following coordinates: x, λ, y (x,y are the pixel dimensions and λ the wavelength). Each pixel can be then analysed at several wavelengths or all pixels at one specific wavelength. These spectels will be used to detect and map the clouds. There about 9 Martian Years of data available, which correspond to approximately 1.4 billion pixels to analyse.

OMEGA characteristics

Concerning the acquisition modes, they are different according to the considered channel. For the visible band, it is a *pushbroom* mode, that is to say that the data are acquired on a two-dimension CCD (Coupled Charge Device), whereas the C and L channels use a *whiskbroom* mode, meaning that the data are acquired simultaneously point-by-point for each spectel and stored on a CCD (Coupled-Charge Device). The width of the scan (or the scan speed) is not the same for each session (16, 32, 64 or 128 pixel columns), it obviously

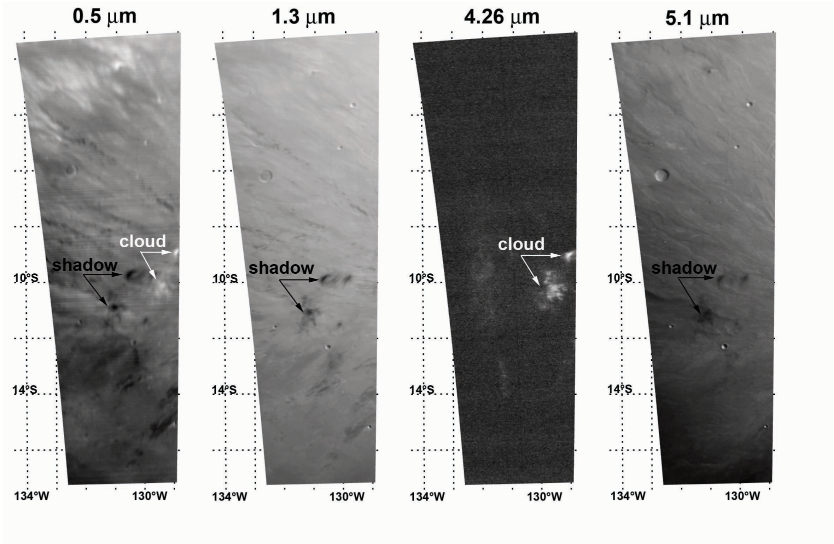

Figure 4.3: Image of a mesospheric CO_2 cloud and its shadow with OMEGA [3].

depends on the satellite altitude: the higher the satellite is, the lower the spatial resolution will be (from 300 m to 3 km per pixel).

Finally, as already mentioned in Section 4.1.1, the Mars Express orbit is very particular. It is indeed very eccentric and nearly polar. This enables to have a large and varied dataset in terms of season, spatial resolution and local time.

Geometry of OMEGA observations

The geometry of OMEGA observations is shown in Figure 4.4. The pointing and the position of the cubes are calculated and registered together with the spectral data for each OMEGA cube as well as the latitude, longitude, solar longitude and local time (but these are not indicated in the figure).

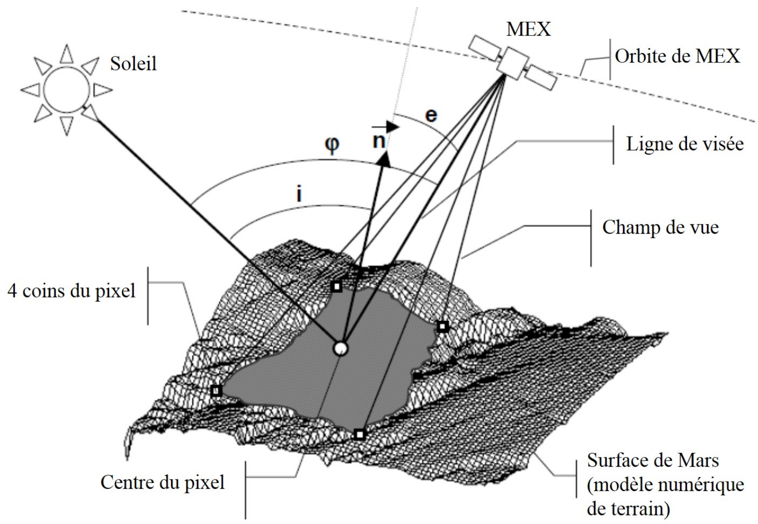

Figure 4.4: Geometry of OMEGA observations: $\vec{n}$ is the normal to the surface, i is the incidence angle between the sunlight and $\vec{n}$, e is the emergence angle between the reflected sunlight and the satellite and ϕ is the phase angle between the sun and the satellite [18].

OMEGA measurements

As already mentioned, OMEGA is an imaging spectrometer. It measures the incident light coming from the martian surface and atmosphere by assessing the number of photons for each wavelength. The raw OMEGA data is then a measure in Digital Units (simply "DU" in the the following). A transfer calibration function is thus defined (see Section 4.2.2) to obtain the raw data in SI units. The radiometric measurement at a specific wavelength is called the energetic luminance (or radiance) I(λ) in $Wm^{-2}sr^{-1}\mu m^{-1}$. It is the sum between the direct reflected and diffused sunlight on the martian surface and the emitted radiation by the surface. It is defined by the following equation:

$$I(\lambda) = H_{aerosols}(\lambda) H_{atm}(\lambda) r(\lambda) \frac{F_{\odot}}{D^2_{Mars}}(\lambda) \cos i + H^{'}_{aerosols}(\lambda) H^{'}_{atm}(\lambda) \epsilon(\lambda) I_{Planck}(\lambda, T)$$

where:

- H_{atm} and $H^{'}_{atm}$ are the atmospheric contributions (absorption and scattering)
- $H_{aerosols}$ and $H^{'}_{aerosols}$ are the aerosol contributions (absorption and scattering)
- r is the surface reflectance
- ϵ is the surface emissivity
- $\frac{F_{\odot}}{D^2_{Mars}} \cos i$ is the solar radiation effectively arriving at the top of the martian atmosphere ($F_{\odot}$ is the solar radiance, D_{Mars} is the Sun-Mars distance and i is the incidence angle seen in Figure 4.4)
- I_{Planck} is the radiance of a black body at a temperature T given by Planck's law [6]

4.2.2. Calibration & Data processing

Calibration

This instrument has to be calibrated before any observations. The radiance I(λ) (see previous Section) is directly related to the raw measurement thanks to the following relation:

$$I(\lambda) = \frac{idat(\lambda)}{F_{calibration}(\lambda)}$$

where:

- idat is the raw data
- $F_{calibration}$ is the transfer calibration function

The dominant source of noise here is the read noise, fixed at 1.85DU (idat raw data units) by the OMEGA team for every spectel [19]. It can be directly linked to the raw data and then help to define the signal-to-noise ratio (SNR):

$$SNR = \frac{idat}{1.85}$$

At the beginning of each orbit around Mars, OMEGA measures the radiometric response to a calibration light (that is a lamp inside the instrument) called OBC (for "On-Board Calibration"). This calibration has been done on Earth before the launch [19] to give a reference measure level to OMEGA. This level should not change because the flux from the lamp is constant (the lamp's age does not have a significant influence on this value). However, due to unknown thermal-mechanical issues, the mirror of the telescope for the infrared channel of this instrument shifts, causing a variation in the incident flux. Thus, as already mentioned in order to use the observations from OMEGA, a transfer function has been implemented to calibrate the data with respect to the reference level measured on Earth [20]. Basically, it enables to convert raw data coming from the instrument in variables that have a physical sense and that can be analysed afterwards.

This method has been validated by analysing the temperature inside the instrument. The principle is to compare the surface temperature derived at 5 μm (end of L channel where the surface thermal flux is the strongest) with a climate model [21]. The calibration analysis is very important to ensure that the spectels are valid.

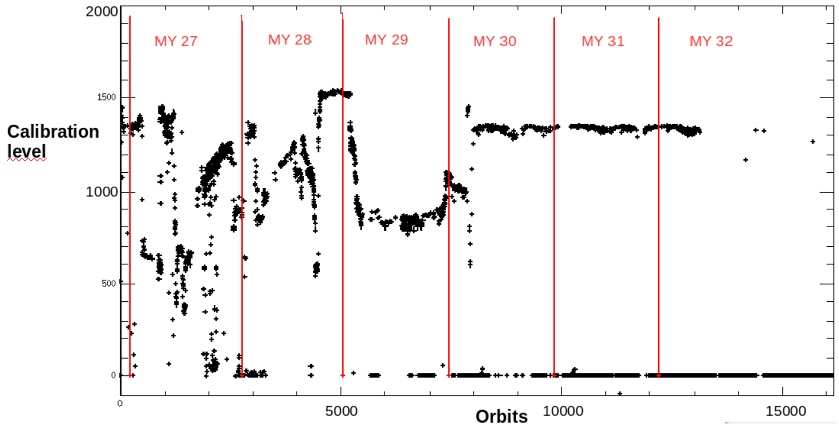

Figure 4.5: Calibration level of OMEGA over the time (the variations are due to unknown thermal-mechanical issues).

However, there are less and less useful data coming from OMEGA. Several reasons may explain this. First and foremost, the calibration level is more and more difficult to adjust due to instrument aging as showed in Figure 4.5. Particularly, there are almost no cubes available anymore at the end of the mission (either the calibration level is too low or the L-channel is not even working). On top of this, the Figure 4.6 confirms that, starting from the orbit 9000, the new cubes contribute to a very low proportion of the whole available dataset.

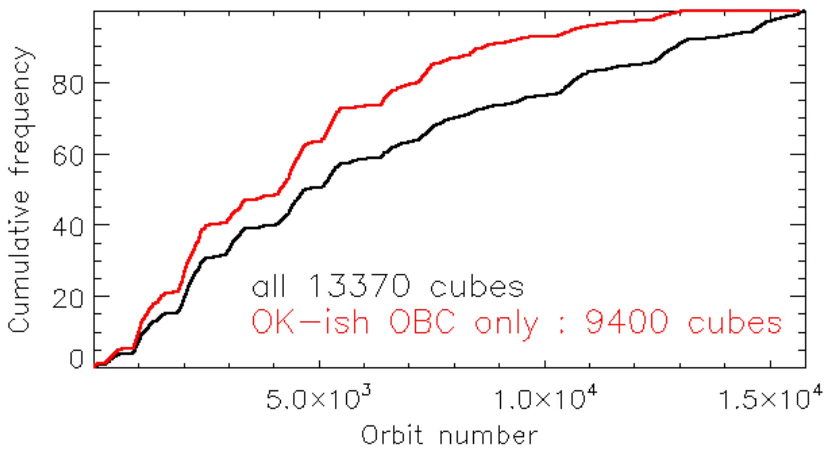

Figure 4.6: Cumulative frequency of OMEGA orbits: it shows that, starting from the orbit 9000, the new cubes contribute to a very low proportion of the whole available dataset.

Finally, the data from the infrared channel are more and more scarce in the recent years. The L-channel, which is necessary to detect the clouds, is less used by the instrumental team because it must be cooled sufficiently when the OBC is measured. Some orbits do not fulfil this condition and hence the corresponding data cannot be included in our study. The infrared channel needs indeed cryocoolers and after nearly 15 mission years, the remaining fluid level is low so it needs to be spared. More and more spectels also do not work anymore due to instrument aging but also cosmic (X-)rays as Mars does not have a magnetosphere. Indeed, it is the magnetic field that protects a planet from these strong energetic rays that may have a violent impact on satellites (and human beings by the way). The figure 4.7 shows the consequences of these phenomena. The reason for the steep decrease of available spectels around orbit 8500 is unknown.

As a consequence, there are between 4 to 5 times less data for the Martian Years (MY) 30, 31 and 32 (that I will analyse) than for the MY 27, 28 and 29. There are indeed about 8200 available cubes in total but only 1500 for the three last years. Besides, among these data, only a small proportion is really treatable. This is a very important point because it is obviously more difficult to detect clouds if the available cubes are less numerous. The criteria to conclude if a cube is useful or not are described in the following. In Figure 4.6, the

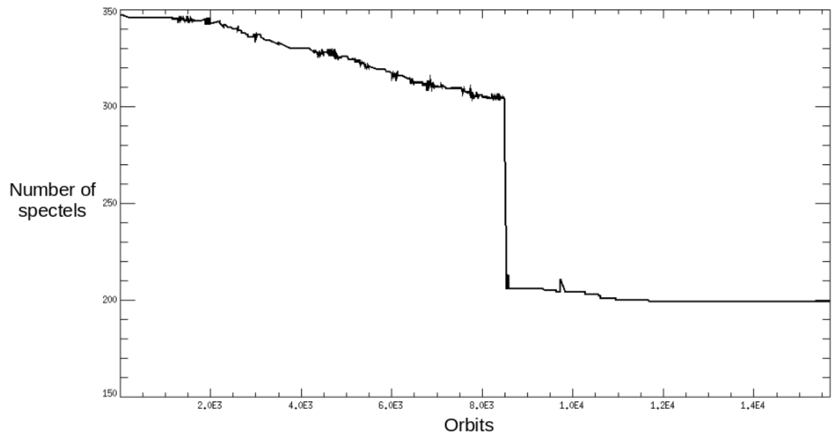

Figure 4.7: Number of available spectels over the orbits (and so the time): the fluctuations are due to spectels which malfunction.

total number of good cubes was about 9400 but when we remove the data without the good pointing (nadir) or the good detector temperature, we then obtain a dataset composed of 8200 cubes.

Data processing

After the calibration and so after obtaining the image at several wavelengths, a data processing is applied to remove all the pixels that are considered to be 'wrong' and thus caused false detections. Some pixels may indeed react differently in terms of temperature and signal-to-noise ratio. As a consequence, a filter has been implemented to determine if a specific pixel is valid or if it should be deleted. This filter as well as its criteria are described below in details. If too many pixels are deleted from the image (the limit has been empirically set to 70% meaning that if more than 70% of the pixels are declared 'bad', then the image is removed from our observations), then the cube is automatically removed from the list. At the beginning, the limit was 50% but I realised that it was too high as it prevents me to detect some clouds. In the following, the different steps of the filter are described, each one enabling to delete 'bad' pixels:

First filtering Before starting to study the whole dataset, some cubes are removed at the beginning because they do not respond to certain criteria, which are describes here. First of all, if the L-channel, which is the channel used to detect CO_2 clouds, is not on, the orbit is not selected. It may seem restrictive as a cloud may be also detectable in the visible channel but two reasons explain this choice. First, even if a cloud is present, in the visible channel, we cannot determine the composition of a cloud, and will thus not be able to distinguish a water ice cloud from a CO_2 ice cloud. Second, there is a lot of work to do in oder to process the whole dataset so this enables to remove a small part of cubes and focus on the others. Another criterion concerns the line of sight of the instrument. At some orbits, the satellite observed the martian moons, Deimos and Phobos, instead of the Martian surface, then these orbits obviously have to be removed. Besides, the instrument sometimes observes Mars at the limb so these orbits are also removed because the detection method (see Section 5.1) cannot work in this case. Finally, the last criterion looks at the detector temperature before the observation. If the temperature is too high, then the orbit is removed because the data measured during the observation may be completely wrong as it is not possible to correctly calibrate the detector.

Pixel removal When the whole dataset has been selected, a pixel filter is applied to remove from the image every pixel that may affect badly the observation. When looking at the signal at 4.24 μm to detect CO_2 clouds, it is very weak as the atmosphere is almost fully opaque so the noise will have a bigger influence at this wavelength band. As a consequence, it is very important to delete any suspicious pixels that could potentially makes the signal 'false'. The major required conditions are listed below:

- **Incidence and emergence angles**: If these angles are too high (more than 110° for the incidence and/or 35° for the emergence), it implies that there is almost no sunlight and so that it will be impossible to correctly observe the surface and the signal at the CO_2 absorption band will be too weak to detect a cloud. We do keep some observations at twilight (incidence angle >90°), since the high-altitude clouds can be illuminated even if the surface is not.

- **Signal-to-noise ratio**: If the signal-to-noise ratio is too weak, it will be impossible to properly observe the image. The minimum has been taken to be 3, which is the limit to easily detect a cloud.
- **Detector temperature**: The temperature of each pixel is also studied to ensure the validity of the signal coming from it. The maximum temperature has been set to -180°C by the instrumental team.
- **Deletion of the first and last pixel lines**: Due to the calibration, the first and last pixel lines (about a dozen for each) of the detector are removed for each wavelength in order to ensure the validity of the results. Indeed, these lines may be corrupted and so 'contaminate' the whole image.

Short-circuit During my thesis, a new electronic problem was discovered in OMEGA. Actually, there is sometimes for unknown reasons a short-circuit during the calibration of the visible channel, which influences the infrared channels. Basically, when the instrument records the images at the visible wavelengths, the electrons inside are not able to evacuate from the detector. As a consequence, a persistent information is still present when the detector tries to capture the cube at infrared wavelengths as the same CCD is used for the visible and infrared channels. This affects the first lines of the detector. It is for this reason that it is sometimes possible to see the surface on the first detector lines at 4.24 μm whereas the atmosphere should be opaque. The problem here is that the algorithm detects a 'cloud' for these cubes because there is a lot of signal due to this electronic issue. To remove all these false detections, a condition about the voltage of each pixel has been implemented to ensure the validity of the signal. When this problem comes, the relative voltage values are indeed completely abnormal (it indicates -10000V whereas the nominal pixel voltage is between -15V and 15V). Consequently, by removing an indicated number of pixel lines for each cube, the false cloud detection is avoided.

All these steps enable to avoid false cloud detections and so save time when searching for CO_2 clouds. However, the different filters described previously do not have an impact on the results given in [5] for the MY 27, 28 and 29. Section 5.3 will show that the previous list of clouds was found by both the detection method and eye-check of the whole dataset. However, the results of this section will help to analyse the new orbits as only the algorithm described in Section 5.3 will be used to detect the clouds now.

4.3. HRSC

HRSC is an imager also on-board Mars Express. The particularity of this instrument is that it takes highly resolved pictures of the martian surface and the atmosphere. By combining OMEGA with HRSC, the detection of CO_2 ice cloud in a HRSC image can be confirmed (see Figure 4.8). Moreover, this imager looks at the clouds with two filters whose lines of sight are slightly different. This geometry enables to determine for instance the altitude and the speed of the clouds by taking images at slightly different times [22]. We have access to those images and we will try to use them as much as possible. They are very interesting because if an HRSC image looking at the same location as an OMEGA session is available, we will be able to visualise the cloud in context (form and structure). It must be noted that HRSC cannot distinguish water ice clouds from CO_2 ice clouds. Thus, the images coming from HRSC have to be correlated with the OMEGA observations.

4.4. SPICAM

SPICAM (SPectroscopie pour l'Investigation des Caractéristiques de l'Atmosphère de Mars) is also a spectrometer on-board Mars Express analysing UV and IR wavelengths [23]. However, in stellar and solar occultation modes on the contrary of OMEGA, it does not analyse the incident light but gives the atmospheric transmission with respect to the tangential altitude (see Figure 4.9). The observations are done as follow: SPICAM targets a reference star (measuring a reference value) and when the spacecraft orbits around Mars, the instrument measures the light from this star through the atmosphere and then does the ratio between these values [2]. This instrument will not be used for our analysis but it may help to obtain further evidence about the source of the condensation nuclei for CO_2 clouds (see Section 7.2).

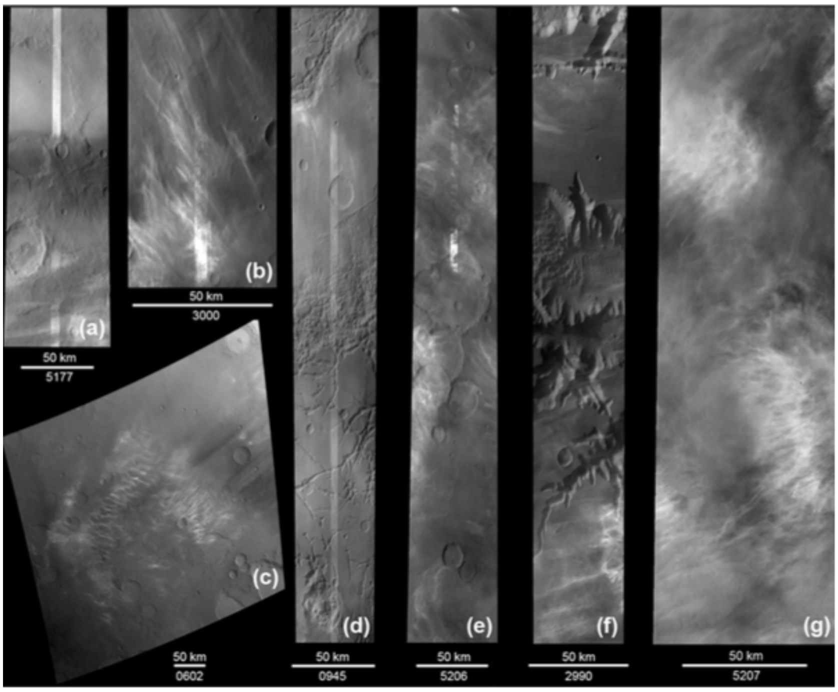

Figure 4.8: Images of mesospheric clouds with HRSC, with four simultaneous observations by OMEGA seen as narrow bright stripe in the middle of the HRSC image ((a), (b), (d) and (e)) [5].

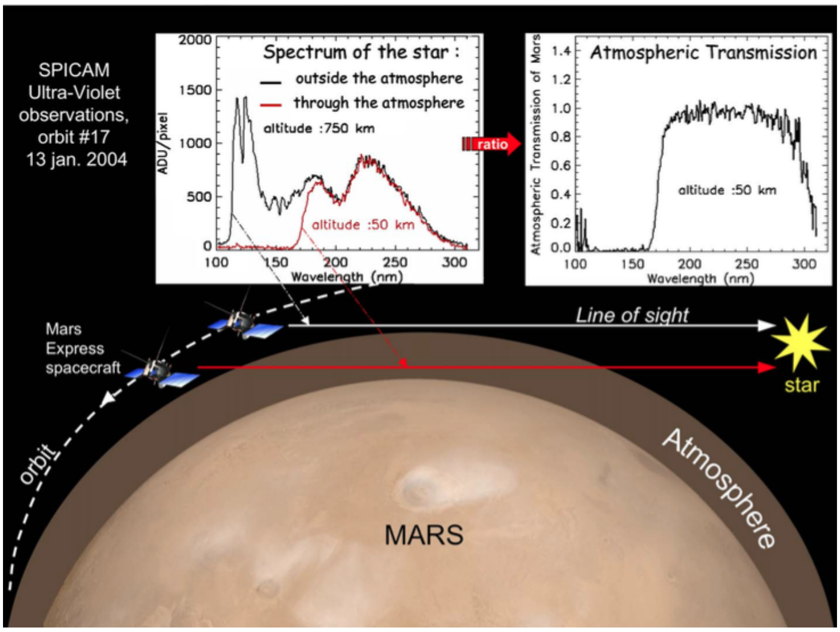

Figure 4.9: Sketch of SPICAM measurements: the instrument measures the atmospheric transmission with respect to the tangential altitude by doing the ratio between the solar spectra inside and outside the atmosphere [2].

5

DETECTION METHOD

In this chapter, the algorithm used to detect the CO_2 ice clouds will be described as well as its limits and improvements to avoid false detections. Moreover, a correlation analysis between the CO_2 ice scattering peak and the visible channel of OMEGA will be conducted in order to try to improve the detections. Finally, the previous list of clouds will be analysed to ensure that the method is valid.

5.1. STATISTICAL METHOD ENABLING CLOUD DETECTION

5.1.1. DETECTION METHOD

This method has been implemented in [5] using the observations from OMEGA to detect and map the clouds. As already explained, the CO_2 ice causes scattering peaks on the spectrum of the reflected sunlight by the surface at certain wavelengths. Particularly, there are two peaks that may be observed in the long-infrared: the first at 4.26μm, which reveals the presence of a cloud, and the second at 4.32μm, which may reveal properties (size of the crystals, optical thickness...) about the cloud itself [3]. An example of such a spectrum is given in Figure 5.1.

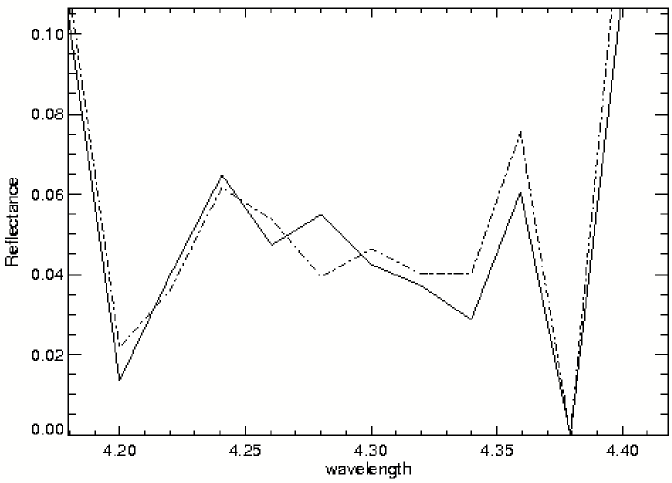

Figure 5.1: Spectra obtained from OMEGA with the cloud detection method for the orbit #7537_4: the solid line shows one spectral peak at 4.24μm and the dashed one shows two peaks, the second at 4.30μm.

However, noise, due to external light or caused by the instrument itself (dark current for instance), could perturb the observations and the fluxes observed. As a consequence, a method has been established to remove this noise as much as possible. The problem is that the noise will be different according to the considered spectel (see Section 4.2). It is for this reason that the method defines a threshold for the clouds for each particular spectel and removes the noise from the signal. This method uses a 3σ limit by considering the noise as Gaussian. Its mean value and variance are derived with an iterative process.

Basically, the so-called local mean value and variance of each spectel in the band is computed (m_{local} and σ_{local}) for the whole cube. Considering that the average variance of the noise should be identical for each wavelength, a mean variance can be computed as well (σ_{global}). This value is then re-used in the calculation of the new local mean value and variance at 4.26μm (wavelength corresponding to the presence of a cloud) by removing all the data above $3\sigma_{global}$. With an iterative process, the 'true' mean value and variance of the noise can be found. Then the pixels with a signal inferior to this level are removed from the observations, enabling to map the clouds [5]. Nevertheless, this method has limits for instance if the cloud signal and the noise can not be statistically differentiated (i.e. if the cloud signal is too faint) or if the cloud is only present in a few number of spectels. This is the method I am going to use in this project to detect and map the CO_2 ice clouds on Mars. An example is given in Figure 5.2.

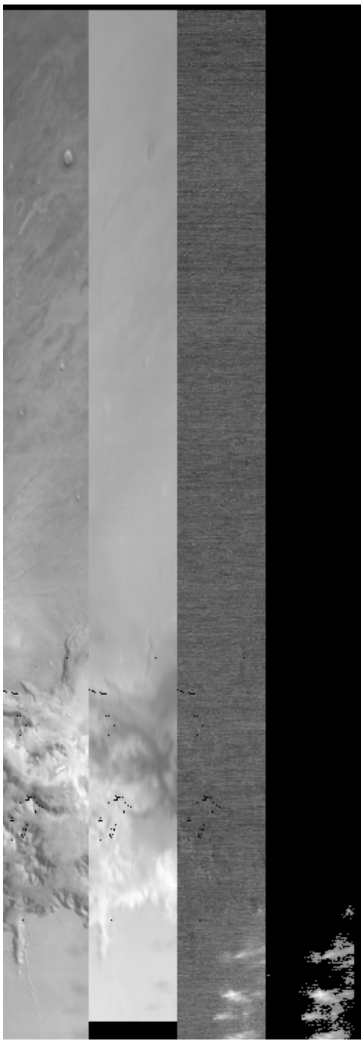

Figure 5.2: Images taken by OMEGA at several wavelengths for the orbit #7537_4: on the left is the image at 5.089μm, then it is the image at 0.489μm, after is the image at 4.24μm in which the cloud is much more conspicuous and finally on the right is the image obtained with the detection method in which the noise has been removed. The black lines correspond to deleted pixels due to OMEGA calibration. This detection has been validated by [4].

By assuming the background noise distribution inside a cube to be Gaussian, the remaining cloud signal above 3σ can be easily extracted, and we have also tested fitting a Gaussian to the cloud signal (see Figure 5.3).

The final goal of the method is to give a certain number of "cloudy" pixels over the total number of pixels containing in the cube because, when the noise is removed from the image, the only pixels left are the ones

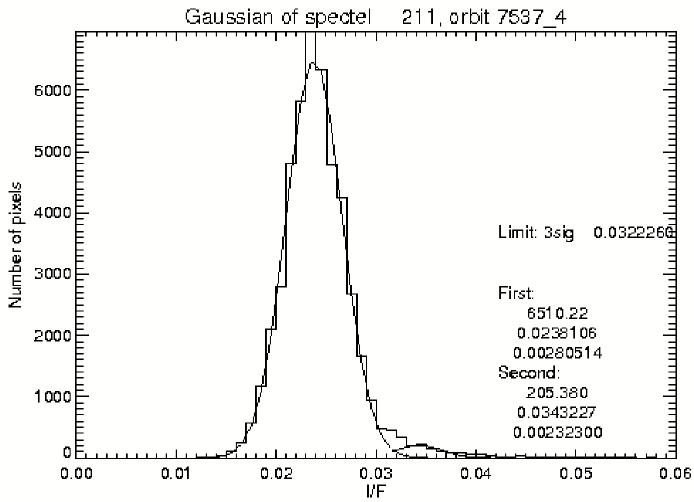

Figure 5.3: Example of the reflectance distribution at the cloud wavelength for the orbit #7537_4. By assuming the background noise distribution inside a cube to be Gaussian, the remaining cloud signal above 3σ can be easily extracted (second peak in the distribution).

with a signal superior 3σ. Moreover, a *match* method has been set to avoid false detections. The previous method indeed computes the number of cloudy pixels at $4.24\mu m$ and at $4.26\mu m$ (because both are inside the CO_2 ice absorption band) and then retains only the common cloudy pixels between them. It ensures that the considered pixels are good. Finally, a method has been implemented to delete the isolated pixels that are identified as cloudy (see Section 5.2.2) because a cloud should have a particular structure of several pixels grouped together. Eventually, one can obtain the total number of cloudy pixels in an image. If this number is greater than an empirical threshold (in our study, we take it equal to 5 regardless the spatial resolution), then it can be considered that a cloud is present inside the cube. It means that if there are at least 5 detected cloudy pixels in the image, then the orbit will be analysed further. However, this method is not sufficient. Actually, the detection algorithm processes every orbit and then returns a list of those that may contain a CO_2 cloud. It is thus necessary afterwards to analyse each of them in details (by watching the image at different wavelengths and the spectrum) in order to definitively conclude about the presence of a cloud or not. As a consequence, the detection method just enables to make a first sorting of the orbits.

5.1.2. LIMITS OF THIS METHOD

As already mentioned, the method described in section 5.1.1 is really interesting because it will enable us to detect most of the clouds. However, it has limits that are important to understand in order to be aware of the fact that some cubes will have to be analysed further to fully conclude about the presence of a cloud or not. These limits are listed in the following:

- If the cloud signal and the background noise cannot be statistically differentiated, the algorithm may not be able to detect the cloud as it will remove all the cloudy pixels from the image. It may be the case, if the instrumental noise is too strong or if the cloud is optically too thin.
- If the cloud is too small (only a small number of pixels on the image), then the algorithm will remove the cube because it does not contain enough cloudy pixels.
- It may happen that, for an unknown reason, the cloud is observed at $4.24\mu m$ but not at $4.26\mu m$ and conversely. In this case, the *match* method will delete all the cloudy pixels.

As a consequence, it is possible that some clouds may not be detected among the whole dataset. However, this concerns a very small number of clouds so it does not impact our results.

5.1.3. USE OF HRSC

As already said in Section 4.3, it is possible to use the HRSC images to confirm the presence of a cloud. Some computer algorithms are indeed available to read these images and extract their geometry. It will enable us to see all the context and structure of a cloud. The problem here is the time of measure. On every orbit, OMEGA indeed observes Mars for about an hour, whereas HRSC is only used for a few minutes as it needs more data storage and energy. As a consequence, even with both instruments observing during the same orbit, it can be difficult to find simultaneous OMEGA and HRSC images looking at a CO_2 cloud.

5.2. IMPROVING THE METHOD

5.2.1. CORRELATION WITH THE VISIBLE

A method to improve the detection and the removal of the noise could be to correlate data coming from several wavelengths. As already mentioned, CO_2 clouds are observed thanks to the scattering peak at 4.26μm but they may be also observable in the visible (see Figure 4.3). The idea is to use the data also in the visible band to detect the clouds. The current method may indeed have difficulties to separate the noise and the cloud signal, particularly if the latter is weak because the detection method will remove all the cloudy pixels in the image in this case. The goal is to analyse the reflectance at a visible wavelength (if a cloud is present during a session, then it can sometimes be observed with the eye). A problem may occur if the surface brings too much noise (because of the presence of ice for instance) and if the surface albedo varies too much but it might help detect more clouds. Four different studies to try to deduce a correlation with the visible band have been conducted. The first one consists in analysing as much cubes as possible on the whole planet with and without clouds in them. This will enable to do a *global* investigation and study of the mean spectrum and see if there are differences when a cloud is present. The disadvantage will be, as already mentioned, that the Mars surface is really different from one cube to another so its contribution in the visible channel will vary and will be difficult to assess correctly. The second method will be to do a *local* study by taking a particular cloud that has been detected at a precise location on Mars and finding every cube that observes that region. Thanks to this, it will be possible to analyse the same location with and without a cloud, which may help to deduce a specific variation at a visible wavelength. Then, a study will be performed by making the noise level vary. As a consequence, noise will be added to the cloud signal to conclude about its effect or not on the reflectance in the visible band. Finally, a statistical correlation function will be implemented in order to analyse the influence of the CO_2 ice absorption peaks on the visible band. These four methods will be studied further in the following.

Global study

In this section, several cubes containing clouds will be analysed in order to try to deduce a *global* correlation between the visible band and the CO_2 ice absorption peak at 4.24μm. The major problem here will be the surface albedo that varies a lot on Mars and so to assess its effect over the mean spectra coming from the cube.

Figure 5.4 presents the values density of blue over red ratio for 4 cloudy (CO_2) orbits: it means the ratio between the reflectance in the blue band (around 0.40μm) and the reflectance in the red band (around 0.75μm).

Figure 5.4 shows that the values taken by the blue over red ratio are generally rather small but with a large orbit-to-orbit variation. Indeed, none of the cloudy orbits has a similar behaviour. Complementary figures are given in Appendix A. There is no common behaviour so it is impossible to efficiently correlate the visible channel with the presence of a CO_2 cloud. The surface albedo may cause these variations. As a result, we cannot conclude anything about a correlation with this method.

Local study

As the previous section showed, a global investigation is difficult because of the surface albedo, which is different for each cube. This is why a *local* study will be performed. The probe Mars Express indeed observes the same region every 11.5 orbits. Of course, there are not always cubes available for each orbit but, as there are 8000 cubes in the whole dataset, I have been able to find an orbit containing a cloud and 4 others observing the same region but without a cloud (#479_3, #1404_3, #4604_4 and #4615_4). This has been possible thanks to the software JMARS from NASA. The reflectance for each orbit has been plotted in Figure 5.5, the black line is for the cloudy orbit #501_2 (considering just the cloudy pixels inside) and the coloured lines for the others.

Again, it appears to be very difficult to deduce any correlations from this figure. Figure 5.6 shows the same graph but only in the visible channel this time.

As for the previous section, it is actually impossible to make any conclusions about a correlation between the presence of a cloud and the signal in the visible band, even if the effect from the surface albedo is removed.

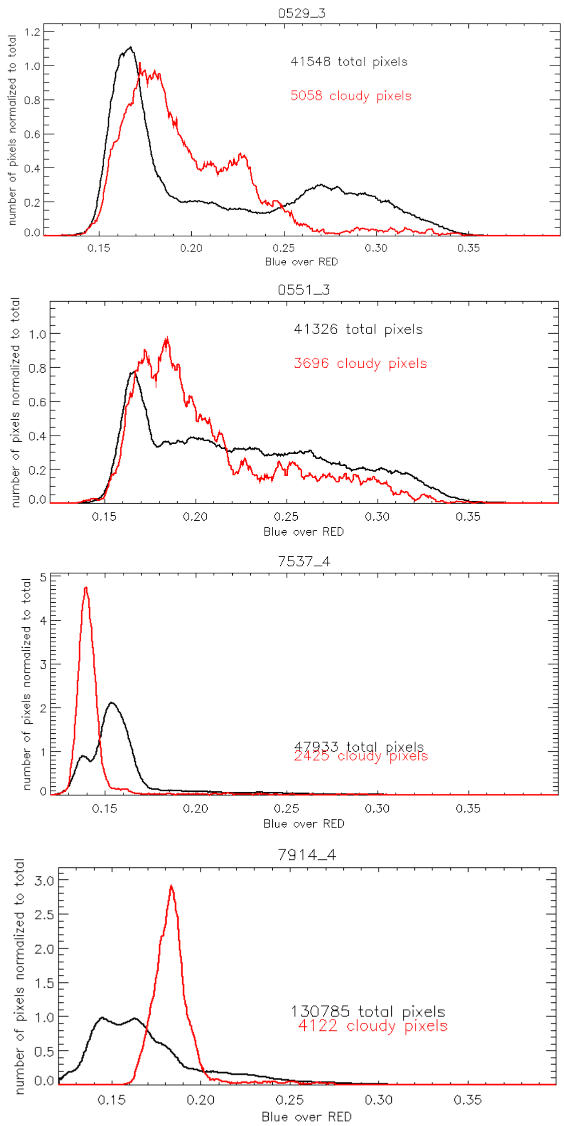

Figure 5.4: Density of values of blue over red reflectance ratio for several cloudy orbits: on the top is the orbit #0529_3, then #0551_3, after #7537_4 and finally #7914_4. The dark curve is the mean reflectance of all pixels of the image and the red one only considers the cloudy pixels.

Noise study

The goal here is to allow more noise in the cloud analysis in order to see if it may help determine a correlation with the visible channel. The usual noise level is set to 3σ but we will study the reflectance for different values (1σ, 1.5σ, 2σ, 2.5σ and 3σ). By adding more and more pixels to the cloud, we hope to find a tendency in its reflectance, particularly in the visible channel. The associated reflectance for each of these values has been plotted in Figure 5.7.

Figure 5.8 shows the same graph but this time only in the visible channel.

As a conclusion, the noise level does not have any impact on the reflectance variation. Each plot has the same behaviour and the slope between the red band and the blue band in the visible is roughly the same.

Correlation function

Finally, a statistical correlation function has been implemented in order to analyse the influence of the CO_2 ice absorption peaks on the visible band. Indeed, as CO_2 may be detected at several wavelengths in the infrared (2.7μm and 4.24μm for instance, see below), we can expect a correlation with the visible. This function is defined as follows:

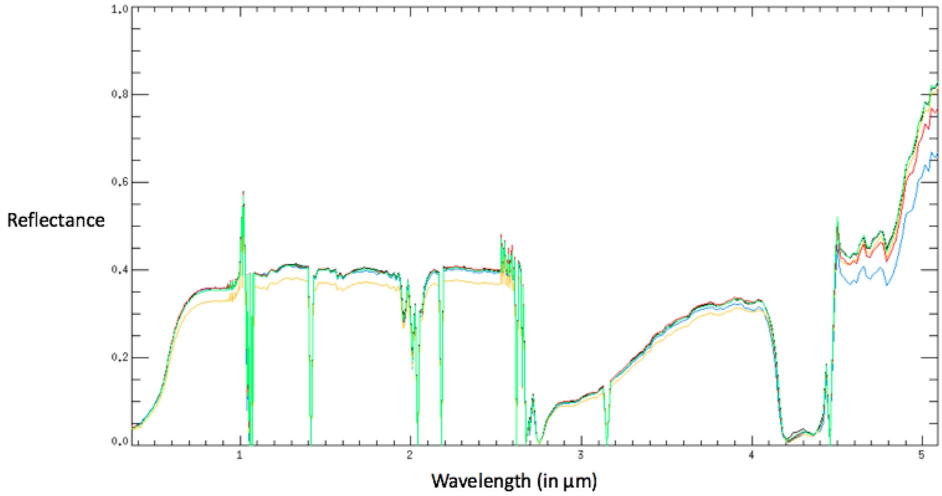

Figure 5.5: Mean spectrum from 5 cubes (only 1 has a cloud inside): the reflectance in black is for the cloudy orbit and in colours the others.

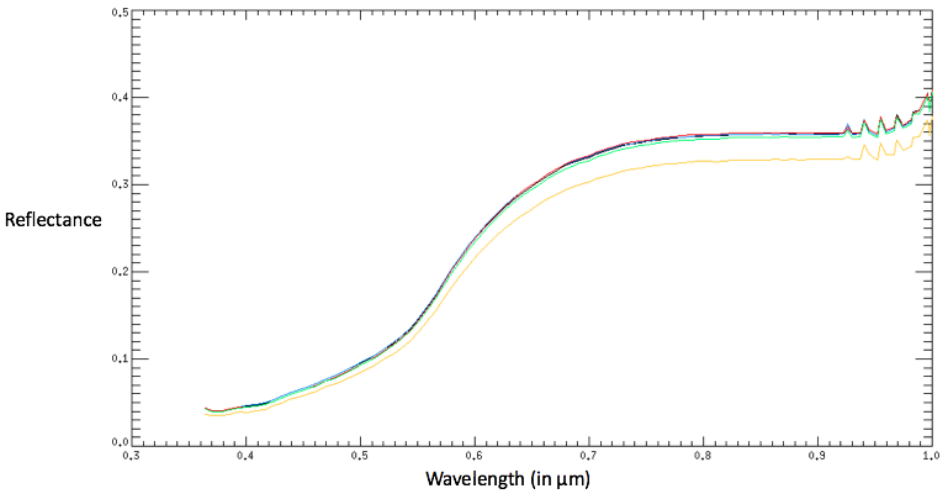

Figure 5.6: Mean spectrum from 5 cubes (only 1 has a cloud inside) over the same region on Mars in the visible channel: the reflectance in black is for the cloudy orbit and in colours the others.

$$M_{corr}(\lambda) = \frac{cov(X(\lambda), X(\lambda_{cloud}))}{\sigma_X(\lambda)\sigma_X(\lambda_{cloud})}$$

With λ_{cloud}=4.26μm, X the reflectance of each pixel of the image, σ the mean reflectance of the image and *cov* the covariance between the signal at 4.26μm and the signal at each other wavelength.

It is possible then to plot this correlation matrix for different cubes with respect to the wavelength and so conclude about a possible correlation with the visible channel. Two examples are showed in the following: Figure 5.9 shows this function for the cloudy orbit #0485_3 and Figure 5.10 for the non-cloudy orbit #4665_5.

This analysis has been done for every cloudy orbit and some other orbits without clouds (the function has also been plotted for other orbits that can be found in Appendix B) and absolutely no conclusions can made as the results depends essentially on the surface albedo, which is almost different for each cube. All the figures show that the results are completely variable from one cube to another even if they all contain a CO_2 cloud. There is a peak of correlation around 2.7μm but it cannot be used as OMEGA spectral sampling is not good enough [3]. Thus, the correlation function does not allow us to link the visible channel with the CO_2 scattering peak.

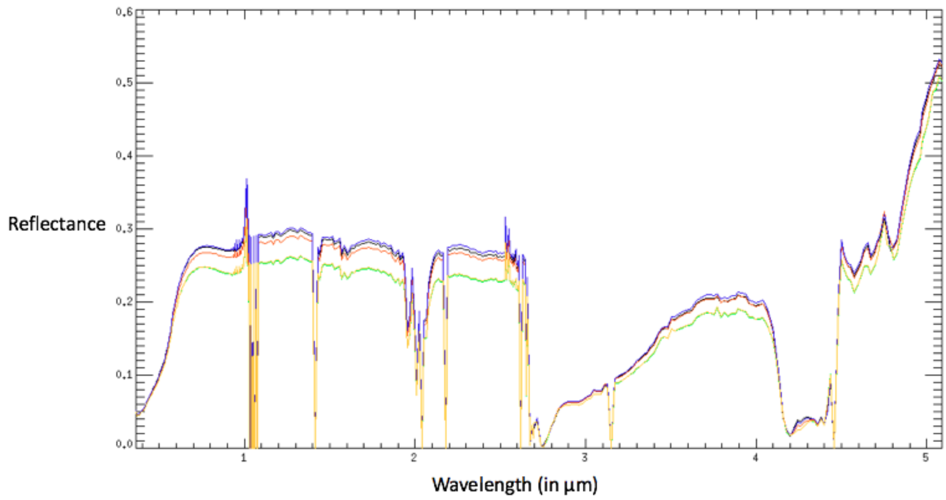

Figure 5.7: Mean spectrum from the orbit #485_3 for different noise levels: 3σ in black, 2.5σ in blue, 2σ in red, 1.5σ in green and 1σ in yellow.

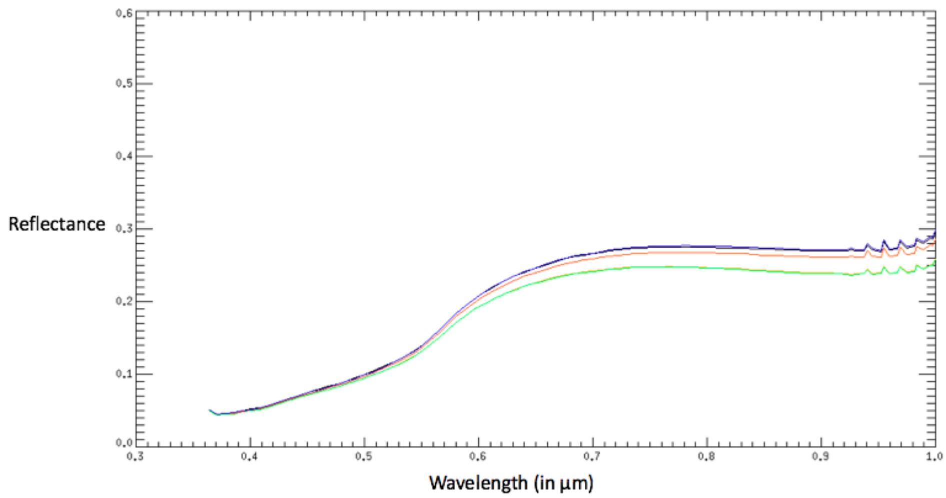

Figure 5.8: Mean spectrum from the orbit #485_3 for different noise levels in the visible channel: 3σ in lack, 2.5σ in blue, 2σ in red, 1.5σ in green and 1σ in yellow.

Conclusion

As a conclusion of this section, unfortunately, it is not possible to correlate the signal from the cloud in the visible channel with the spectral peak around 4.24μm. Four different methods have been studied in detail but none of them have been conclusive. Two causes may explain that. On the one hand, the surface albedo of Mars probably varies too much to make any global conclusions. On the other hand, the previous results may strongly depend on the characteristics of the CO_2 cloud itself. The results may indeed change according to the size, shape and optical thickness of each cloud as our results are very different from one cloud to another. For these reasons, the detection method cannot be improved by using the signal in the visible channel.

5.2.2. REMOVING ISOLATED PIXELS

As described in Section 5.1.1, the detection method returns a certain number of cloudy pixels, and if this number is large enough (5 in our study), it may indicate the presence of a CO_2 cloud inside the cube. However, it is important to remove all the isolated pixels before making any conclusions about the detection of a cloud. It has indeed a particular structure. If the cube is composed of several cloudy pixels distant from each other, it cannot be considered as a cloud. Consequently, these pixels have to be deleted in order to avoid false

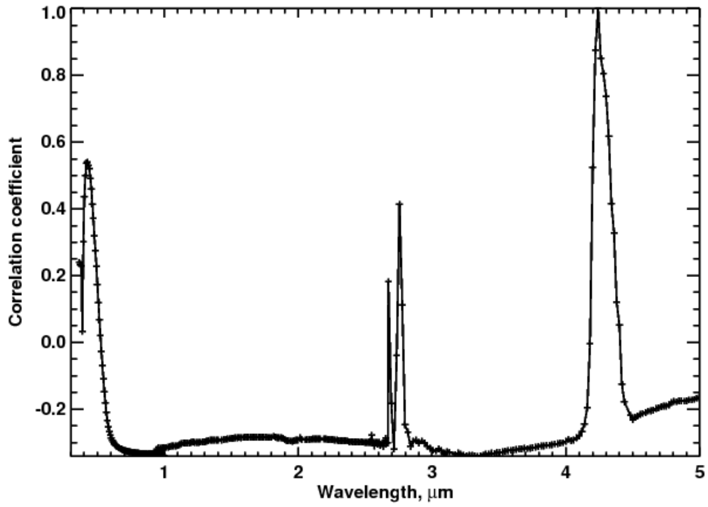

Figure 5.9: Correlation function for the cloudy orbit #0485_3 between the 4.26μm image and the image collected at all other wavelengths.

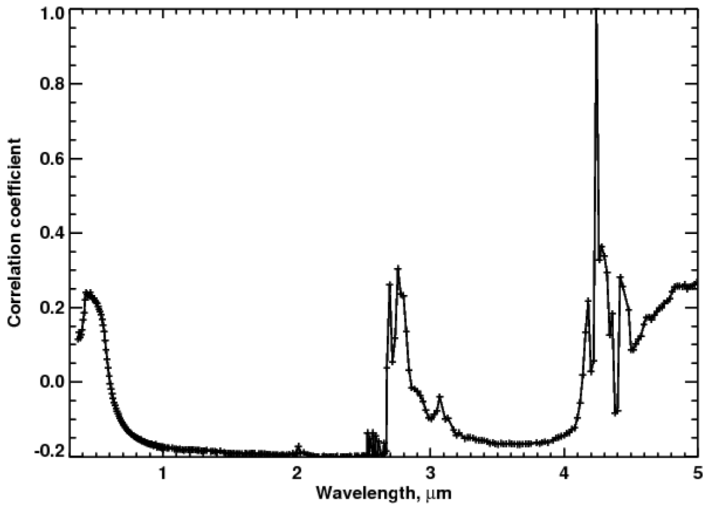

Figure 5.10: Correlation function for the non-cloudy orbit #4665_5 between the 4.26μm image and the image collected at all other wavelengths.

detections. The method developed by [5] includes that kind of script but only for the pixels close by. It means that if a cloudy pixel is not attached to another one, it is then removed from the detection. However, a cloud cannot be composed of only 2 pixels in our case. It it why this script has been improved by enlarging the number of pixels to study around a cloudy pixel (48 vs 9 previously) as well as the required number of cloudy pixels around to keep it (5 vs 1 previously).

5.2.3. FALSE DETECTIONS

Thanks to the methods described in Sections 4.2.2 and 5.1, it is possible to analyse all the data coming from the OMEGA instrument in order to detect the clouds. However, a phenomenon of instrumental aging starts appearing around orbits 7500-8000, which is almost exactly the beginning of Martian Year 30. As a consequence, more and more data are corrupted and then cannot be analysed with our method or give rise to a large number of false detections. In the following, some insights to avoid these false detections are given.

Dead pixels

As already explained in Section 5.1.1, the detection method consists in evaluating the noise level for a certain spectral band (typically between 4.2 and 4.4μm) and only keep the signal above 3σ. By taking into account several wavelengths, the noise level is smoothed and enables a better detection. However, according to Section 4.2.2, the number of available spectels decreases with respect to mission time due to instrument aging. It is why in Figure 5.1, the reflectance is equal to zero at 4.37μm: this spectel is unfortunately "dead". This has a great impact because, when the algorithm assesses the noise level, its variance may be completely wrong as the signal coming from the considered spectel is unrealistic. As a consequence, a lot of false detections occurred because of this. These "wrong" cubes contain indeed, according to the method, more than 50% of cloudy pixels, which is completely aberrant. It is why it has been decided to limit the detection method (and so the evaluation of the noise level) at only the signal at 4.24 and 4.26μm. Thanks to that, the obtained results are far more coherent.

Volcanoes

There is another source of false detections due to the topography of the martian surface. The Figures 5.11 and 5.12 enable to have a better look on the situation. More particularly, Figure 5.11 is a re-projection of the data in three colours. It uses three visible bands: in red is the band (0.729μm, 0.737μm, 0.744μm, 0.752μm, 0.759μm), in green is the band (0.603μm, 0.610μm) and in blue is the band (0.416μm, 0.424μm, 0.431μm. By superposing these three images, we can add more context and better visualise the data on the planet. This orbit is actually observing the volcano Olympus Mons.

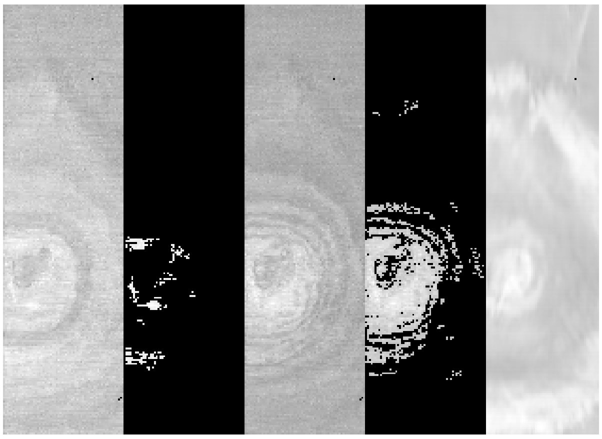

Figure 5.11: Images taken by OMEGA at several wavelengths for the orbits #8653_4: on the left is the image at 4.24μm, after is the image obtained at 4.24μm with the detection method in which the noise has been removed, then is the image at 4.26μm, after is the image obtained at 4.26μm with the detection method in which the noise has been removed and finally on the right is the image at 0.489μm. The black lines correspond to deleted pixels due to OMEGA calibration.

The method seems to detect a cloud and we can observe something in the images when the noise is removed. In fact, the re-projection of the image enables to perfectly see a cloud around Olympus Mons. However, the structure in circles is very particular at 4.24μm and 4.26μm for a CO_2 cloud. It seems that OMEGA observes the martian surface whereas the atmosphere should be completely optically thick at these wavelengths. This is a very particular case because the blue form on Figure 5.12 is actually a cloud but a H_2O one, which is really confusing for our study. We know it is a water ice cloud by calculating a water index using the reflectance at 3.38μm and 3.52μm and basically computing the ratio between them [21]. Moreover, it is possible to observe something at this orbit but when we look at every orbit that flies over Olympus Mons or other volcanoes on Mars, it is not always the case. Section 6.1 will help to understand this phenomenon and how to avoid it.

Lack of signal

Finally, due also to the aging of the instrument, the signal may not be very good, particularly in the CO_2 ice absorption band. The atmosphere is indeed optically completely thick at these wavelengths so the signal that arrives at OMEGA is very small. Because of the aging of the instrument, its sensitivity has decreased and such small signals appear to be hard to detect. As a consequence, some cubes are impossible to analyse. Two examples are given in Figure 5.13.

Actually, these cubes may be useful as it is possible to analyse them in the visible channel. However, the signal in the infrared is completely noisy and impossible to study with the detection method. Even if a cloud is observed in the visible channel, it would be impossible to conclude about its nature (H_2O or CO_2).

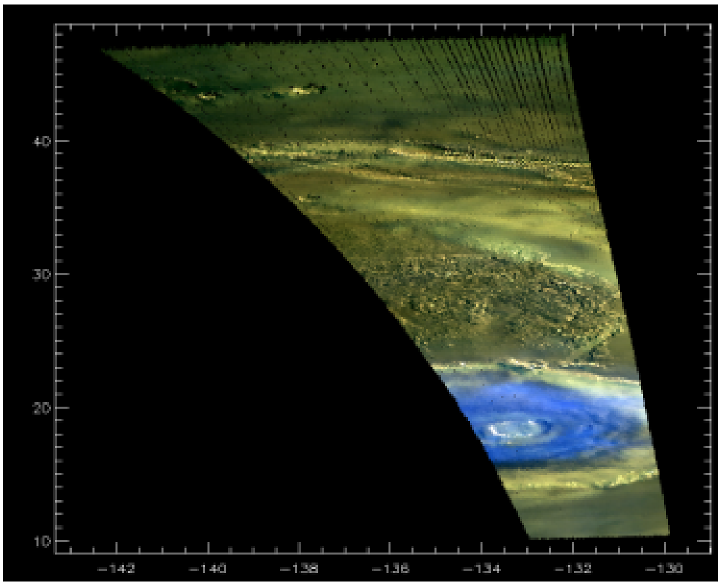

Figure 5.12: Re-projection of the image (latitude vs longitude) in RGB (Red-Green-Blue) of 3 visible bands for the orbit #8653_4: in red is the band (0.729μm, 0.737μm, 0.744μm, 0.752μm, 0.759μm), in green is the band (0.603μm, 0.610μm) and in blue is the band (0.416μm, 0.424μm, 0.431μm). In blue, a cloud is visible around Olympus Mons.

5.3. PREVIOUSLY DETECTED CLOUDS

A first list of 64 mesospheric CO_2 ice clouds has been published in [5] as well as some of their characteristics. Besides, HRSC images were used to confirm the detection. However, these clouds were not only found thanks to the method described in Section 5.1.1 but with the help of engineers (particularly B. Gondet) from the OMEGA instrumental team who checked each cube by eye. The first goal was to ensure that the detection method works well and that it was able to find all the clouds in the list. Almost all the clouds are detected as the images are very clear (see Figures 5.14 and 5.15).

However, some of the clouds in the list were more difficult to detect (for instance, the cubes #0430_2 or #0997_6) because the clouds are very thin and are composed of only a very small number of pixels. Consequently, in order to find them, the detection threshold has to be decreased (2σ for these cases with respect to the standard 3σ). Finally, some clouds are not found because, for unknown issues, they are detectable at 4.24μm and not at 4.26μm and inversely (for example the cube #0945_6). As already mentioned in Section 5.1.1, a match method is implemented to only retain the cloudy pixels found at both of these two wavelengths. As a consequence, the cloudy pixels are removed from the image because they are only present at one wavelength. This problem can be solved by also decreasing the detection limit as it enables to increase the number of cloudy pixels.

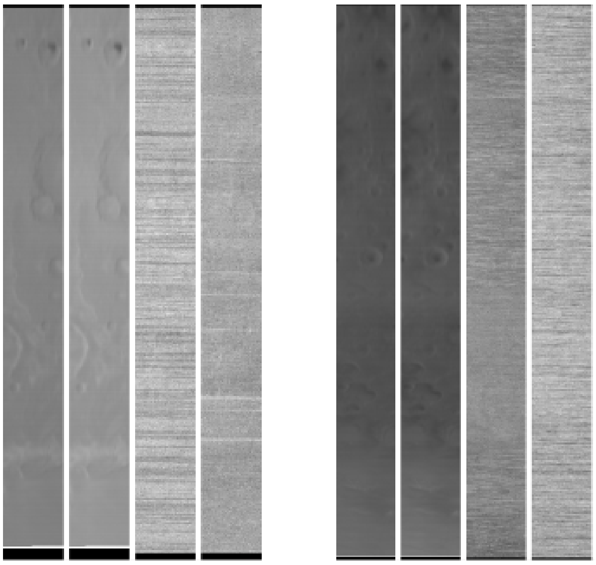

Figure 5.13: Images taken by OMEGA at several wavelengths for the orbits #9535_2 (left) and #B598_2 (right): on the left is the image at 0.489μm, after is the image at 0.618μm, then is the image at 4.24μm and finally on the right is the image at 4.26μm. The black lines correspond to deleted pixels due to OMEGA calibration.

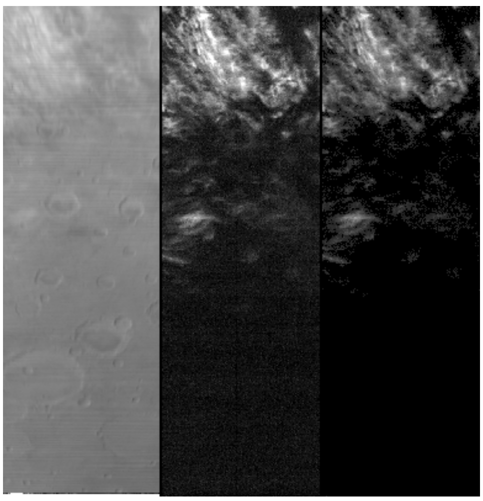

Figure 5.14: Images taken by OMEGA at several wavelengths for the orbit #0485_2: on the left is the image at 0.489μm, after is the image at 4.24μm and finally on the right is the image obtained with the detection method in which the noise has been removed.

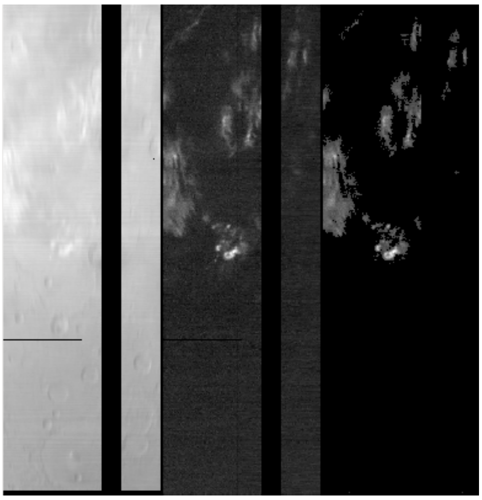

Figure 5.15: Images taken by OMEGA at several wavelengths for the orbit #0551_3: on the left is the image at 0.489μm, after is the image at 4.24μm and finally on the right is the image obtained with the detection method in which the noise has been removed. The black lines correspond to deleted pixels due to OMEGA calibration.

6
Results

6.1. Atmospheric pressure and the volcanoes

As already explained (see Section 5.2.3), it is sometimes possible to observe the martian surface, particularly volcanoes, in the CO_2 ice absorption band whereas the atmosphere should be optically thick (if there is no CO_2 ice cloud) and inhibit OMEGA from seeing the surface. Figure 6.1 enables to understand better why the surface is visible for the orbit #8653_4. Actually, it shows that the maximum signal at 4.24μm is linked to the topography, and more especially with the maximum altitude of Olympus Mons. We may then conclude that if the topography of the martian surface is mountainous, then the signal measured will be higher and so will give the possibility to observe the surface.

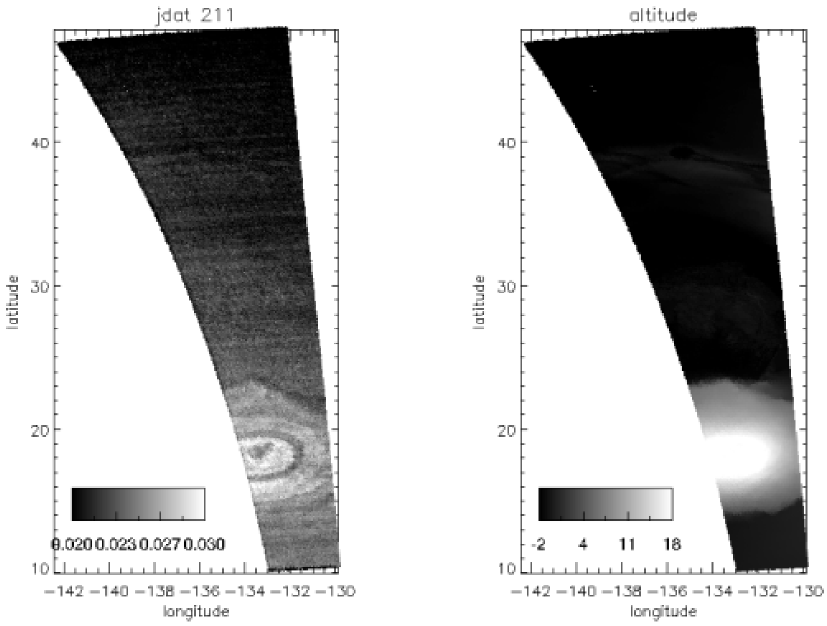

Figure 6.1: Images obtained with OMEGA above Olympus Mons: on the left is the signal at 4.24μm with respect to the latitude and longitude and on the right is the topography of the image. It shows that the maximum signal correlates with the maximum altitude.

The reason here is certainly due to the atmospheric column above the volcanoes, which is less thick than elsewhere. As CO_2 is the major constituent of the martian atmosphere, normally the signal coming from the surface at 4.24μm (and 4.26μm) is completely absorbed. Thus, OMEGA cannot measure it. However, above the volcanoes or high topography (with an altitude superior to 10 km), this atmospheric column is thin enough to enable some photons to reach the instrument. As a consequence, the thinner the atmospheric column is, the more visible the surface will be.

Nevertheless, as already mentioned, it is not always possible for OMEGA to observe the volcanoes. Figure 5.11 shows an orbit in which the martian surface is observed above a volcano, but on other orbits which looks at the same region, it is not always possible to see it. A hypothesis to explain this phenomenon is that it is correlated with the amount of CO_2 in the atmosphere.

In order to demonstrate that, a list of all orbits that pass over a mountain with an altitude superior to 10 km has been established and the signal at 4.24μm has been measured for each of them. It is possible then to do an histogram for all values of signal at 4.24μm with respect to the solar longitude (or season) and the surface pressure and conclude about the season where it is maximum and minimum. As there is a lot of data to process, the altitude of the mountains has been constrained to two intervals: 10-12 km and 12-14 km. Figure 6.2 shows the results of this analysis.

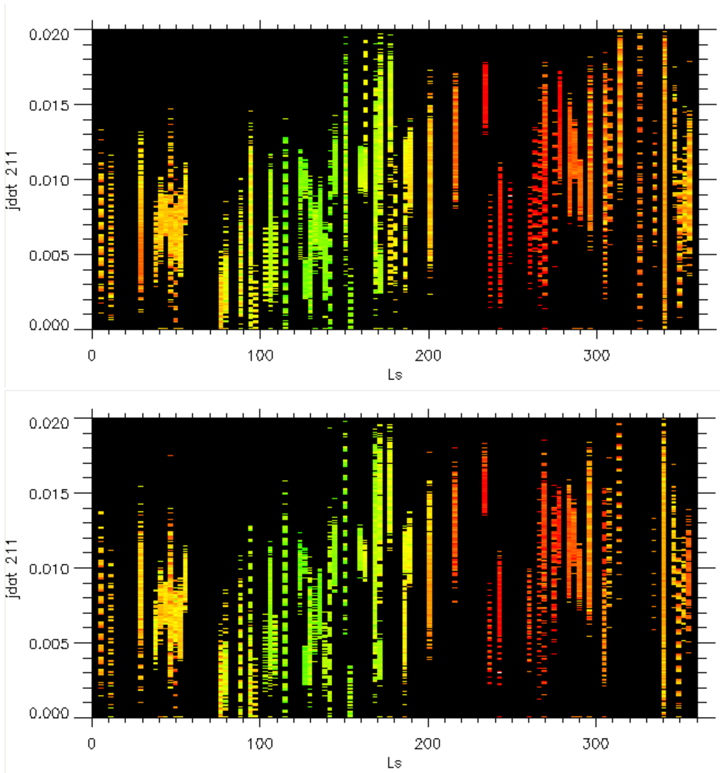

Figure 6.2: Histograms of the radiance at 4.24μm with respect to the solar longitude for the altitude intervals 10-12km (on the top) and 12-14km (on the bottom): the green parts represent the smallest pressure values and the red ones represent the biggest pressure values.

These figures show that the signal at 4.24μm is maximum around Ls=150°-180°, thus it is easier to observe the volcanoes at this period. On the contrary, the signal is less strong around Ls=70°. Now, we can correlate our results with the variation of the surface pressure. Indeed, according to the Viking landers, the surface pressure on Mars over a year varies (see Figure 6.3).

As a consequence, it should be easier to observe the surface of volcanoes if there is less CO_2 in the atmosphere, which happens around Ls=150°. At this period indeed, the signal coming from the surface should be maximum as there is less atmosphere to absorb it. It is exactly what we observed previously. It is also possible to see a correlation between the signal values and the surface pressure around Ls=70°. However, it is much more complicated to conclude for the largest surface pressure values at Ls=240°-270° when the surface should be more difficult to see: further analysis is needed.

As a conclusion, we may say that volcanoes and high mountains on Mars are particularly visible when the surface pressure is the lowest and we are able to detect this tendency in OMEGA data. This explains why some false cloud detections can happen. To avoid this kind of phenomenon, the data coming from pixels with a surface altitude superior to 10km have been removed.

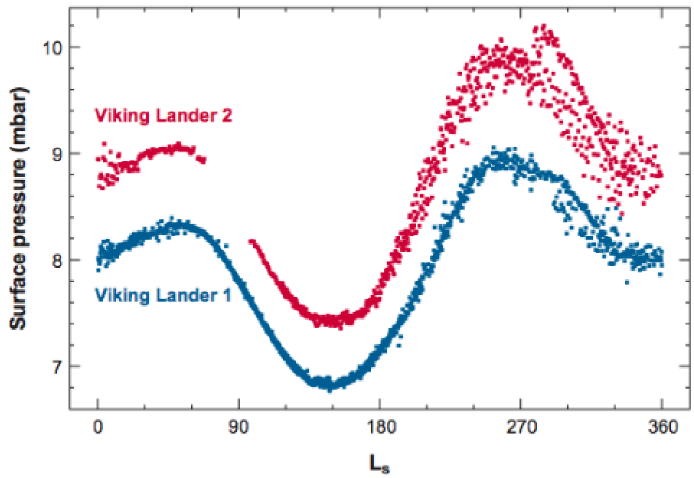

Figure 6.3: Annual surface pressure variation on both Viking landing site (22°N and 50°N). The shift between the two curves is due to a difference of altitude between the two sites (about 1 km) [24].

6.2. NEW DETECTED CLOUDS

6.2.1. LIST OF CLOUDS

The detection method detailed in Section 5.1.1 enables to obtain a first list of possible cloudy orbits. Each of these orbits needs now to be studied further one by one to conclude about the presence of a cloud or not. Thanks to the previous section, it possible to avoid a large number of false detections and so make the search for CO_2 clouds easier. Thus, the presence of all the clouds in the following detected by the method, has been confirmed.

Orbits	Ls(°)	Latitude(°N)	Longitude(°E)	Local Time
7536_3	11.0	2	7.7	13.3
7537_3	11.1	-2	268	13.3
7537_4	11.1	-2	268	13.4
7554_3	13.5	-0.5	353.6	13.2
7604_3	20.3	0.5	351	12.7
7679_3	30.3	2	345.5	13.0
7686_3	31.2	-5.5	359	12.8
7768_3	41.9	4.5	8.5	11.2
7875_4	55.5	4.0	3.5	10.1
7907_4	59.6	-0.5	341	9.72
7914_4	60.5	5.0	356	9.64
7953_0	65.4	7	343	9.3
8020_0	74.0	8	335.5	8.4
8048_0	77.5	3.5	345.5	7.8
8335_0	114.8	-8.0	357.9	17.1
8371_0	119.7	-16.0	275.1	16.6
8395_0	123	-8.5	314.3	16.4
8592_2	151.2	-1.0	349	14.4
A230_0	55.2	-2.5	0.29	7.16
A297_0	63.8	-3	340.1	6.25
A539_0	94.6	-2	290.8	15.8

Table 6.1: List and properties of the new CO_2 clouds found with OMEGA (Orbits, Solar Longitude, Latitude, Longitude and Local Time). The orbit starting with 'A' means '10' (for instance, A230_0 means 10230_0), the letters enable to keep the same structure as for the first orbits.

21 new clouds have been discovered from Martian Year 30 until now. Remembering the fact that there are almost 5 times less data than for the previous study [5], it is a very good number. Some of them (18) have been already published [4]. Table 6.1 gives the full new CO_2 clouds list. Besides, one more cloud shadow has been discovered in orbit #7537_4 (see Figure 5.2, on the bottom). Properties derived from this shadow can be found in Section 6.3.2.

6.2.2. IMAGES FROM HRSC

As described in Section 5.1.3, images from HSRC may be used to confirm the presence of a cloud and observe its structure in a bigger context. They can also enable to compute its altitude and speed. Considering the list of CO_2 clouds found in Table 6.1, HRSC images are available for several same orbits. These orbits and some properties of the image are listed in Table 6.2.

Orbits	Observable?	Latitude(°N)	Longitude(°E)
7537_3	Yes	[53;63]	[265;269]
7768_3	No	-	-
7875_4	No	-	-
7914_4	No	-	-
8371_0	Yes	[-2.8;16.3]	[273;276]
8592_2	Yes	[-46;-30]	[348;351]
A539_0	Yes	[-23;-14]	[290;292]

Table 6.2: List and properties of the clouds found with HRSC for the same orbits as OMEGA (Orbits, Observability, Latitude and Longitude)

Some of the clouds found with HRSC are not "observable". It means that the image is too narrow to actually see something. As a result, this prevents us us to confirm the presence of a cloud for a specific orbit. Moreover, by analysing the common orbits between Tables 6.1 and 6.2, one can conclude that the images from both instruments have not been taken at the same time and location for each orbit. This has been explained in Section 5.1.3. Thus, the clouds observed with HRSC are not the same as the ones observed with OMEGA. As a consequence, we cannot use HRSC images to extract more properties from none of the CO_2 ice clouds on the list found with OMEGA.

6.3. PROPERTIES

In this section, the main results extracted from OMEGA observations will be discussed. First the properties of the clouds will be listed including their location and season. This study will also use the previous results from [5] in order to obtain more statistics. Second, a cloud shadow analysis will be performed to extract new characteristics concerning altitude, optical thickness and particle size.

6.3.1. GENERAL CHARACTERISTICS

General properties of mesospheric CO_2 clouds extracted from [5] and the previous list in Section 6.2.1 are:

- **Solar Longitude (season)**: L_s=330°-80°; 90°-150°; 200°-300°. This corresponds mainly to the northern hemisphere spring and summer for the equatorial clouds and autumn for the mid-latitude clouds.
- **Latitudes**: -25° to 25°N; 50° to 70°S and 40° to 60°N.
- **Longitudes**: -130° to 30°E; 120° to 170°E.
- **Local Time**: From 6 to 18 (clouds form at any moment of the day).

Figures 6.4, 6.5 and 6.6 enable to see the distribution of the clouds over the planet and seasons.

6.3.2. CLOUD SHADOWS

Here, the same analysis as in [5] is performed to extract the optical properties and the altitude of the CO_2 cloud. As already mentioned, a new cloud shadow has been found for the orbit #7537_4.

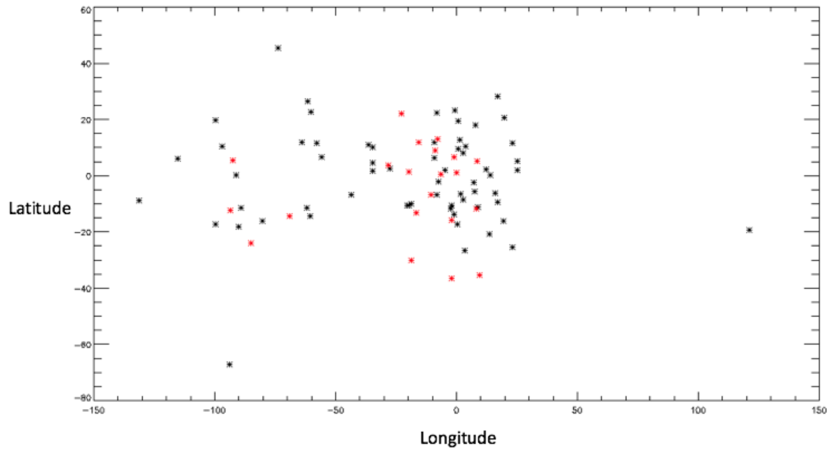

Figure 6.4: Latitude vs Longitude of the mesospheric CO_2 clouds: in black are the clouds found in [5] and in red the new ones.

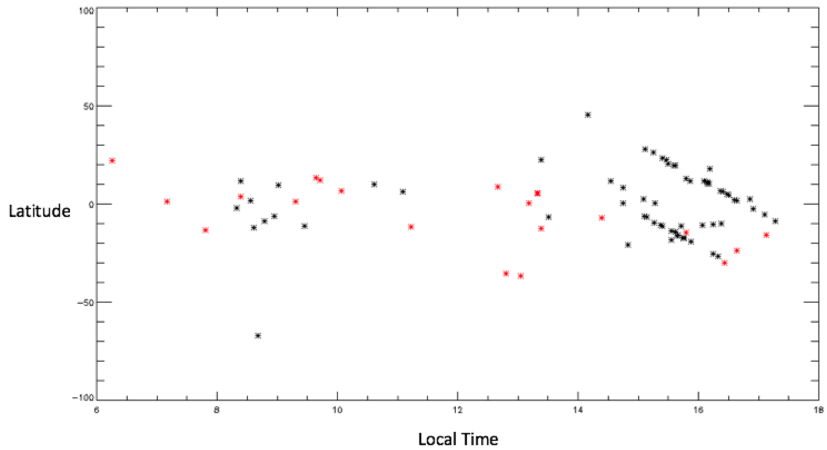

Figure 6.5: Latitude vs Local Time of the mesospheric CO_2 clouds: in black are the clouds found in [5] and in red the new ones. The 'lines' are due to observations biases.

Cloud altitude First of all, thanks to OMEGA geometry described in Figure 4.4 and simple trigonometry, it is possible to assess the cloud altitude by projecting it on the ground and using its shadow. Some hypotheses are required such as:

- The distance between the projection of the cloud and its shadow is small (about 50-100km) to neglect the effect of Mars curvature (otherwise spherical trigonometry has to be used)
- The surface should not have prominent topography

Thanks to these assumptions, we are able to compute the cloud altitude of orbit #7537_4 and we found an **altitude of 73km**. By comparison, the altitude found by [3] for the orbit #0501_2 was 80km. Our result is consistent with the altitude range observed by [9], which was 40-100km.

Indeed, according to radiative transfer modelling [2], in order for the clouds to be detected by the instruments at the CO_2 ice absorption wavelength band, they have to be above 40km. Anyway, the temperatures are too high below this altitude to enable CO_2 cloud formation. Finally, according to [9], it seems that the equatorial clouds form at higher altitudes than the mid-latitude ones. It is the same for clouds forming early in the spring than after.

Optical thickness and particle size In order to determine the optical depth and the particle size with the observations from a spectrometer, two methods may be used: either using a full radiative transfer model to

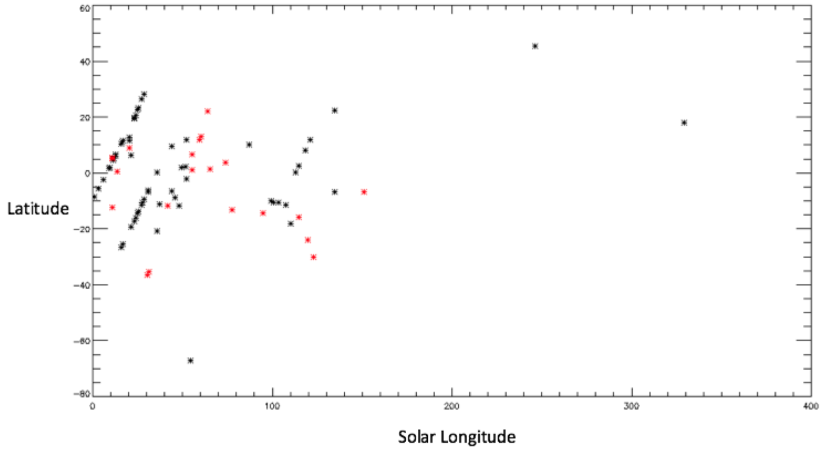

Figure 6.6: Latitude vs Solar Longitude of the mesospheric CO_2 clouds: in black are the clouds found in [5] and in red the new ones.

simulate the observations and finding the best fit of the spectra or if it is possible, using cloud shadows [5]. The latter consists in computing the contrast ratio for the wavelength band 1.0-2.7μm for each pixel (some large absorption wavelengths were removed like at 2.0μm to not perturb the results because the contrast ratio in these bands is too high), then fitting the contrast ratio by adjusting the optical thickness [3].

The formula that enables to compute the optical thickness (τ_c) is as follows:

$$\frac{R_{ish}}{R_{osh}} = \frac{\exp[-\tau_c/\cos\theta] + \frac{F_{dif}}{F_{dir}}}{1 + \frac{F_{dif}}{F_{dir}}}$$

where R_{ish} is the reflectance of the surface inside the shadow, R_{osh} outside the shadow, θ is the solar zenith angle and $\frac{F_{dif}}{F_{dir}}$ is the ratio of the components of the solar flux (diffuse and direct) outside the shadow, which can be determined with OMEGA.

The particle size is then fitting by using Mie theory [3]. The principle is to implement a distribution of CO_2 ice particles with several size (here it is assumed that the particles are spherical) and optical thickness ranges. Then, we can compare the contrast ratio from these simulations and the one from observations. By doing this, it is possible to compute a range of particle size for the CO_2 ice cloud. The results can be found in Figure 6.7. The range for the **optical thickness is 0.004-0.048** and for the **particle size is 0.19-1.84μm**. Both results are consistent with [9] (0.01-0.6 for optical thickness and 0.08-3μm for the effective radius).

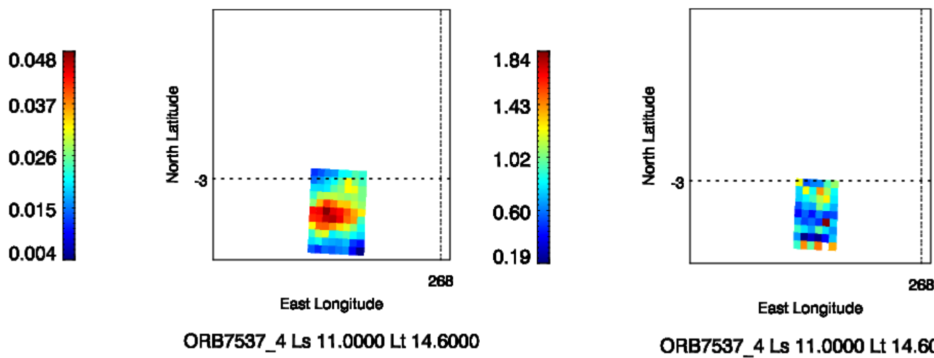

Figure 6.7: Maps of optical thickness and effective radius for the orbit #7537_4: on the left is the optical thickness and on the right the particle size (some pixels have been removed because the results found with the algorithm were clearly outliers).

6.4. SIMULATION OF CLOUD SHADOWS

In order to understand better the properties of the cloud shadows and in which cases they might be observable, a Monte Carlo code has been implemented. This code (in fortran) has been developed by my supervisor at Delft, Daphne Stam, and enables to model the Martian atmosphere into atmospheric layers and send photons to observe the shadow of a cloud present in one of these layers. By doing this, we will be able to conclude about the impact of the cloud altitude and optical thickness on the presence of the shadow, correlate these results with real observations from OMEGA and then determine general properties of the CO_2 mesospheric clouds.

6.4.1. DESCRIPTION OF THE MONTE-CARLO CODE

First, a general description of the Monte-Carlo code will be given to understand the method, its limits and how cloud properties may be extracted from it. As already mentioned, the goal of this code is to compute the appearance of shadows of CO_2 clouds by varying the altitude, the optical thickness, the particle size and the solar zenith angle.

The Martian atmosphere is modelled as a stack of layers and a CO_2 cloud is introduced in one of these layers. The Monte-Carlo code then sends photons to this model and computes their path through the atmosphere using scattering processes. If a photon encounters a cloud particle, it will be scattered (or possible absorbed) and its new direction will depend on the scattering pattern of the cloud particle. Photons can also be scattered by molecules in the Mars atmosphere. Finally, the algorithm records how many photons reach the ground and at which locations. Depending on the characteristics of the cloud (size, optical thickness...), it will limit the number of photons that reach the surface. Thus, we will be able to observe the position of the shadow of the cloud according to the solar zenith angle.

In order to store the number of photons reaching the ground, the top of the atmosphere and the surface are divided into grids with a spatial resolution of 5km. The geometry of the simulation is given in Figure 6.8.

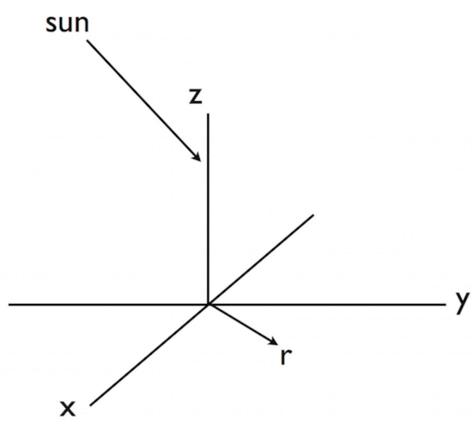

Figure 6.8: Geometry used for the Monte-Carlo code: the Sun is in the yz-plane and the cloud around the z-axis. The cloud is circular, the r-axis defines its radius.

The coordinate system is Cartesian with the xy-plane on the surface and the yz-plane the plane of symmetry. In order to simplify our model, the Sun is in the yz-plane and the cloud is concentrated around the origin (z-axis) so we only need to write out the grid cells along the y-axis in order to determine the extend and depth of the shadow. Besides, there are twice more pixels in the y-direction because the negative x-direction is mirrored to the positive x-direction.

The code takes the following inputs:

- **Cloud bottom and top altitude (in km)**: the top of the atmosphere has been empirically chosen to be at 100km
- **Cloud horizontal dimensions (in km)**: a circular shape is used in our case so we only need to define the radius, the vertical dimension can also be taken into account
- **Optical thickness**

- **Particle size**
- **Cloud particle refractive index**: at the wavelengths where we want to do the computations (in the visible in our case)
- **Solar zenith angle (in degree)**

For each photon that is sent into the atmosphere, the code will do the following:

1. Compute the length of the photon path, which depends on the optical thickness of the layer where the photon is currently in: the larger the optical depth, the shorter the path.
2. If the path remains in the same layer as the photon originally was, it will be scattered. The algorithm then calculates its new direction, which depends on the scattering properties of the particles (gas+cloud particles if present) in the layer.
3. If the path takes the photon into a different layer, it will be released at the top (or bottom if the photon travels upwards) of this new layer and a new travel length is determined based on the new layer's properties. Goto step 2.
4. If the photon was in the highest atmospheric layer and the path takes it out of the atmosphere, it will be lost and a new photon is sent into the model.
5. If the photon was in the lowest atmospheric layer and the path takes it into the surface, it will be lost too but its location is stored.

Results from our simulations are given in the following section.

6.4.2. SIMULATIONS

In this section, the results from the Monte-Carlo will be described. First, we will show the nominal simulation for the study and then, we will do a theoretical investigation by modelling the shadow depth as a function of the cloud optical thickness, the cloud altitude and the solar zenith angle. The depth of the shadow is computed as the ratio between the number of photons in the shadow and the number of photons in the surrounding continuum.

Nominal simulation

For the nominal simulation, the following inputs are chosen:

- Altitude of the cloud: 82km
- Vertical size of the cloud: 500m
- Radius of the cloud: 5km
- Optical thickness: 0.4
- Particle size: Power law with a minimum radius of 0.1μm and a maximum radius of 4μm
- Cloud refractive index: 1.0004486 at a wavelength of 0.6μm
- Solar zenith angle: 40°

As already mentioned, the surface is divided into grid cells and we only need to study the ones along the y-axis as the photons are sent in the yz-plane and the cloud is near the origin (see Figure 6.8). The obtained results have been plotted in Figure 6.9.

The same figure has been zoomed in the shadow region in Figure 6.10

The dip around pixel 1000 is the shadow. The location will depend on the solar zenith angle. The shadow is not entirely black: some photons reach the surface because they travel through the cloud or because they are scattered to the region below the cloud. In order to estimate the depth of the shadow, we compute the ratio between the number of photons in the shadow zone and the number of photons outside. As a consequence, the lower the ratio, the deeper the shadow. For the nominal situation in Figure 6.10, we obtain a ratio of 8.07%.

In the following sections, we will study the effect of changing several inputs: the altitude, the optical thickness and the solar zenith angle. By doing this, we will be able to validate the Monte-Carlo code and to understand the impact of these variables on our results.

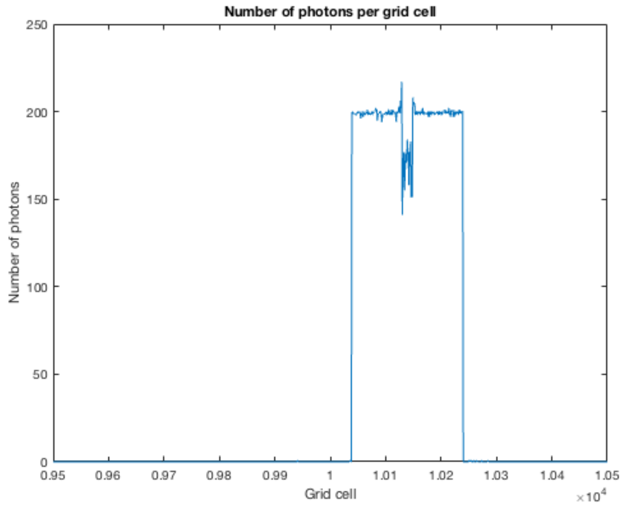

Figure 6.9: Plot of the results from the Monte-Carlo code for the nominal situation: It is the number of photons per grid cell. There are two empty regions because we only send photons near the origin with a certain solar zenith angle so only a little region receives them. The peaks are certainly due to the forward scattering peak of the cloud particles

Effect of the altitude

First, we will plot the results obtained by changing the altitude of the cloud. Originally the cloud has been set at an altitude of 82km. Here, three other altitudes will be studied: 62km, 72km and 92km. Normally, the lower the cloud, the less photons should be scattered to the region below the cloud. Thus, the depth of the shadow as described in Section 6.4.2 is expected to decrease with increasing altitude.

The results for altitudes of 62km, 72km and 92km can be found in Figure 6.11.

For these altitudes, the depth ratios are respectively 7.87%, 8.22% and 7.92%.

We can thus observe that the depth of the shadow effectively increases from the altitudes 62km to 72km but curiously, it decreases after for the altitudes 82km and 92km. It may reveal one of the problem of the Monte Carlo code: the noise. It is indeed very high in our simulations, which may cause these variations. Several simulations should be conducted to try to remove this noise.

Effect of the optical thickness

Second, we will do the same analysis as the previous effect but this time, we will make vary the optical thickness of the cloud. According to Section 6.3.2, the optical thickness of the CO_2 is between 0.01 and 0.57. We will then study three specific values for the optical thickness: 0.1, 0.57 and 5. The last one is just used to validate our results. Indeed, the thicker the cloud, the darker the shadow should be. Thus, the depth of the shadow is expected to increase with increasing optical thickness.

The results for optical thickness of 0.1, 0.57 and 5 can be found in Figure 6.12.

For the optical thicknesses 0.57 and 5, the depth ratios are respectively 7.77% and 2.59%. It is impossible however to assess the depth for the first case.

We can thus observe that for an optical thickness of 0.1 (and below), the noise is too high to correctly observe the shadow. So its depth is really low. On the contrary, for an optical thickness of 5, the shadow is perfectly clear and observable. So the variation of the depth of the shadow with the optical thickness seems good.

Effect of the solar zenith angle

Lastly, we will study the impact of changing the solar zenith angle that is the angle by which the photons arrive on the CO_2 cloud. Three cases will be also studied, which correspond respectively to a solar zenith angle of 0°, 20° and 60°. By making vary the solar zenith angle, the location of the cloud shadow and its surface will change. We would expect a longer shadow with a larger solar zenith angle, thus a lower sun. It should also be deeper because the path through the cloud is longer. On the other hand, the amount of outside light will probably be larger with increasing solar zenith angle.

The results for solar zenith angle of 0°, 20° and 60° can be found in Figure 6.13.

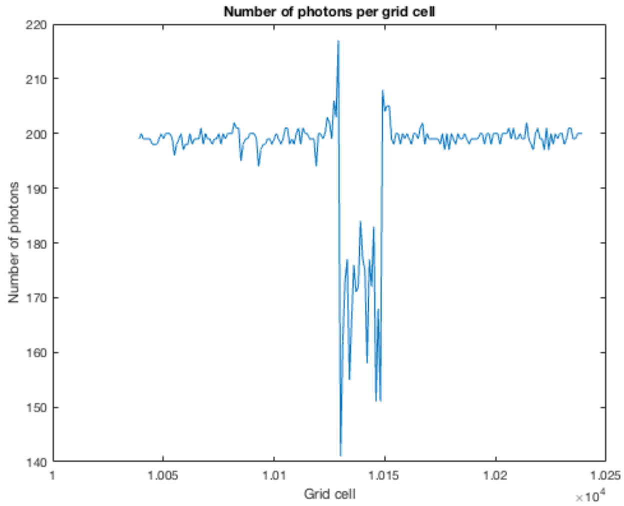

Figure 6.10: Plot of the results from the Monte-Carlo code for the nominal situation in the shadow region: it is the number of photons per grid cell.

For these solar zenith angle, the depth ratios are respectively 8.40%, 7.97% and 6.40%.

Thus, the shadow is very observable for a solar zenith angle of 0° as shown in the top picture of Figure 6.13. It is the best condition to see a shadow. Besides we can see that the depth of the whole shadow zone as well as its displacement from the below the cloud increase with increasing solar zenith angle. These properties are in agreement with our first assumptions.

Conclusion

As a conclusion, we can say that the results from the Monte-Carlo code are consistent with our assumptions. Some results are unreliable but it is due to the high noise that are present in the simulations. In order to have smoother results, we should do several Monte-Carlo simulations with different noises and then take the average. However, our work gives a good basis for further analyses in characterising CO_2 cloud shadows.

6.4.3. PERSPECTIVES OF THIS METHOD

The results obtained in Section 6.4.2 show that the Monte-Carlo code works and makes us able to simulate the shadow of a CO_2 cloud. The next first step would be to model the particle size of the CO_2 clouds and see their impact on the depth of the shadow. It would be also interesting to take cloud properties from SPICAM/OMEGA observations and to test how dark the shadow would be. For instance, by reproducing the shadows in cubes #0501_2, #0551_3 and #7537_4 with the exact same inputs, we will be able to conclude about the validity of our model and if our results are consistent with the ones found in Section 6.3.2. Moreover, by using existing cubes where CO_2 clouds have been detected and observed, we can determine a range of value for their optical thickness, particle size and altitude as their shadow cannot be observed.

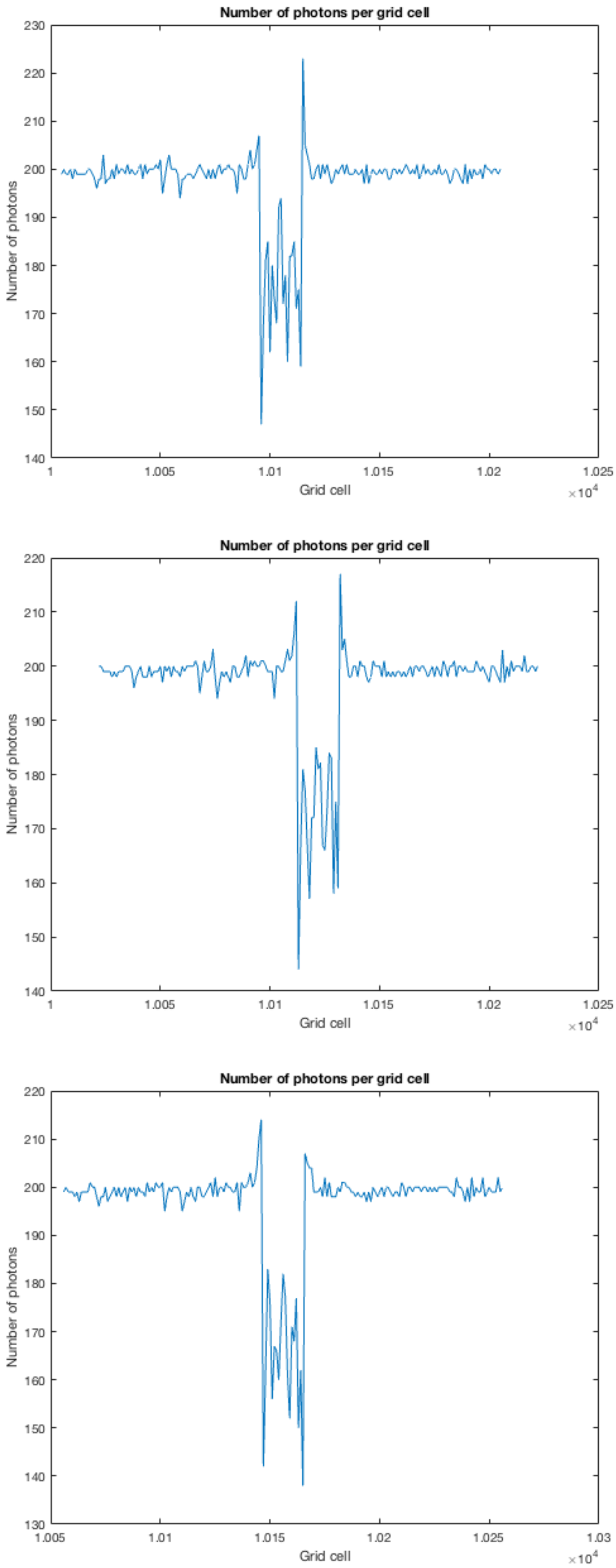

Figure 6.11: Plot of the results from the Monte-Carlo code for three different altitudes in the shadow region: on the top is 62km, on the middle is 72km and on the bottom is 92km. For each figure, we plot the number of photons per grid cell.

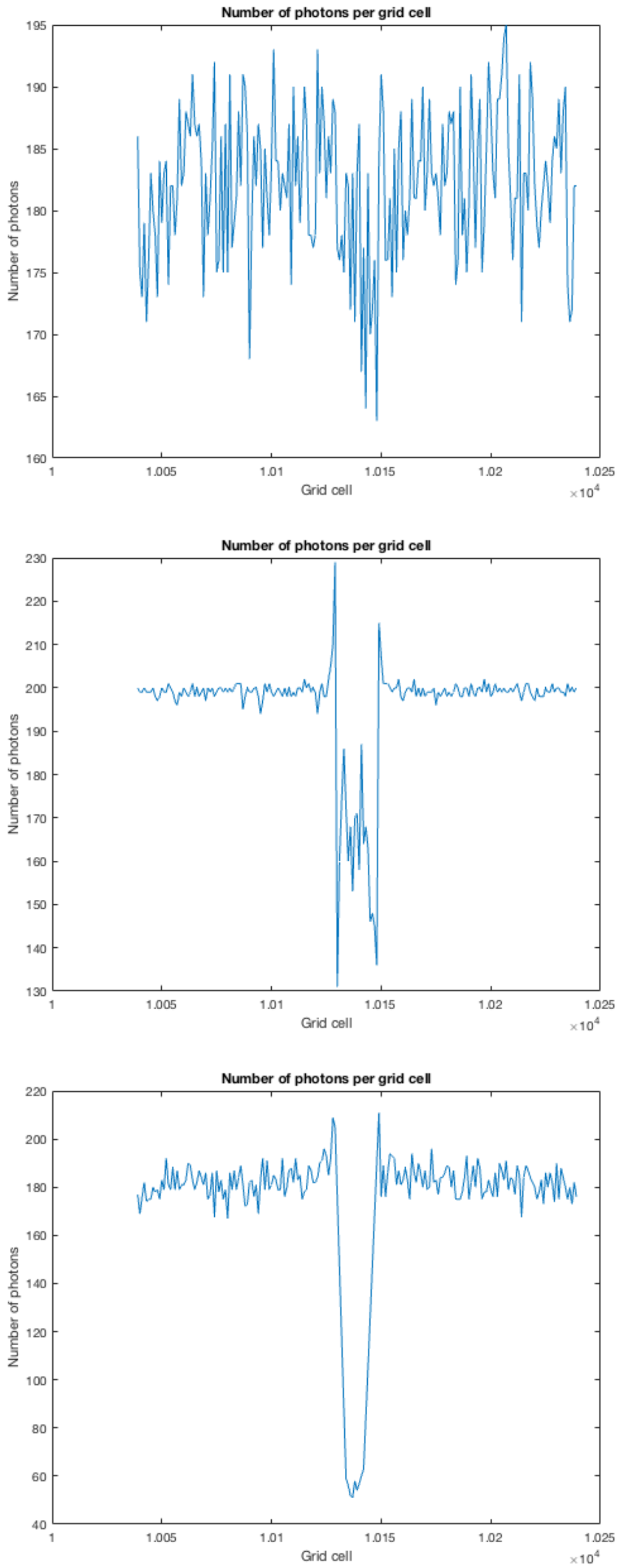

Figure 6.12: Plot of the results from the Monte-Carlo code for three different optical thickness in the shadow region: on the top is 0.1, on the middle is 0.57 and on the bottom is 5. For each figure, we plot the number of photons per grid cell.

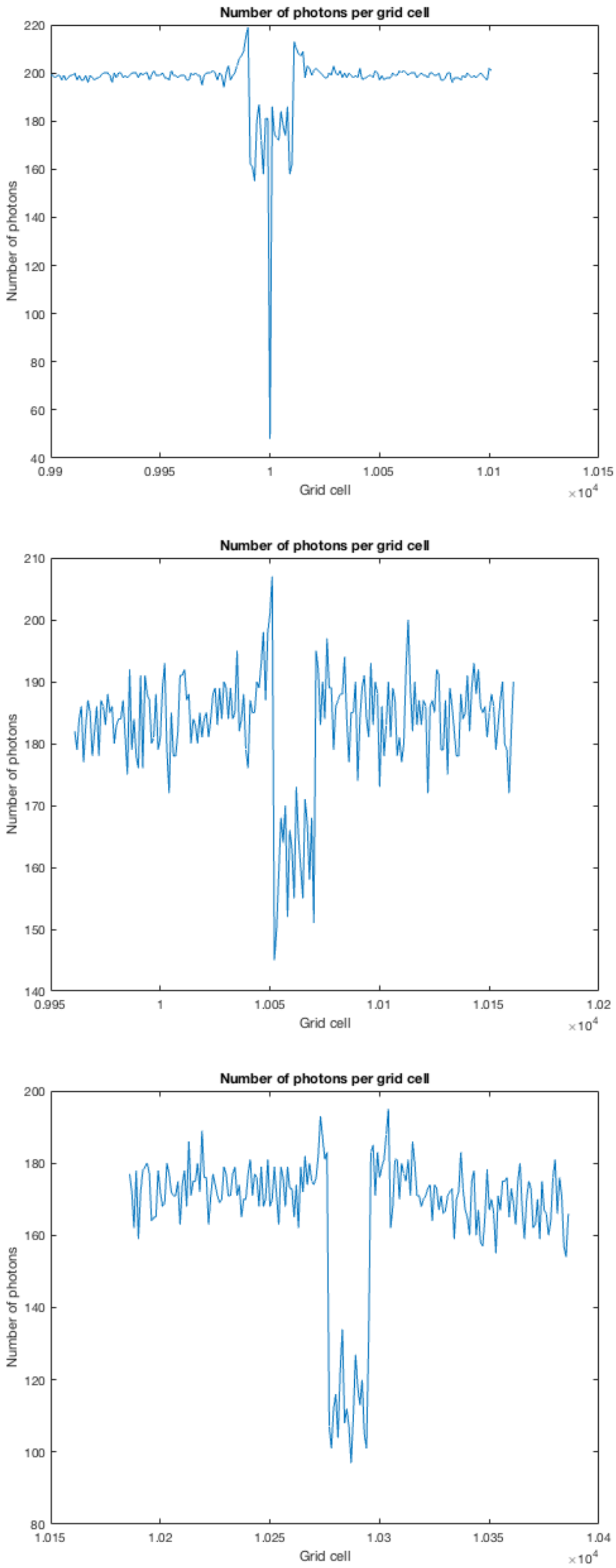

Figure 6.13: Plot of the results from the Monte-Carlo code for three different solar zenith angle in the shadow region: on the top is 0°, on the middle is 20° and on the bottom is 60°. For each figure, we plot the number of photons per grid cell.

7

Formation of CO_2 clouds

7.1. Source of the condensation nuclei

In Section 2.3, possible sources for the condensation nuclei have been mentioned. It was shown that the formation process is supposed to be heterogenous nucleation but there are still doubts concerning the origin of the aerosols that enable the formation of CO_2 clouds. It may be dust or meteoritic smoke. As already explained in [13], dust particles settle very fast and they are probably no longer present in sufficient quantities in the mesosphere during clouds season. Moreover, even if we could observe something with OMEGA, it would be impossible to conclude anything because of observational biases. The time and space coverage are indeed insufficient for the Martian Years 27-29. Finally, it is also difficult to correlate the clouds season with meteoritic smoke as there is a constant layer of it in the mesosphere during the whole year. Actually, it seems to be the local temperature in the mesosphere that really plays a role in the formation process.

We need then long-term and homogeneous observations with (if possible) the same instrument in order to be able to conclude about the possible correlation between dust storms and CO_2 clouds. At the beginning of my thesis, it was hoping to have a lot more available CO_2 clouds observations to compare them with the amount of dust for each year. Unfortunately, we do not have very good statistics and the coverage is insufficient as the L-channel of OMEGA (see Section 4.2.2) is almost dead. Thus, it is difficult to do this comparison. The next section will give some insight and methods that may help to determine the formation process and the source of the condensation nuclei.

7.2. Perspectives

As already mentioned, the small amount of new data from OMEGA prevents us to conclude about the source of the condensation nuclei. In the following, several possible studies that may help to answer this question will be listed.

7.2.1. Use of SPICAM

As explained in Section 4.4, SPICAM is a spectrometer that observes the Mars atmosphere at the limb and assesses the atmosphere transmission with respect to the tangential altitude. This instrument is then able to analyse the aerosol layers in the mesosphere and the particles inside. It is indeed possible to observe smaller particles than with OMEGA. Actually, the objective here is to do the same study as [25] with SPICAM. In this article, the polar mesospheric H_2O ice clouds on Earth have been studied and the source of the condensation nuclei has been described as ice (coming from water ice in this part of the atmosphere) and meteoritic smoke. It has been possible by analysing different types of composition (pure ice or ice plus several kind of smokes), measuring their extinction ratios and comparing them with the observations. It is easier to do this analysis on Earth because there are a lot more available data but it may be possible to do the same on Mars thanks to SPICAM because it works almost like SOFIE instrument, which is used in [25]. As a consequence, by taking several kind of smoke compositions we can find on Earth, we could compare them with observations at Mars limb done with SPICAM and determine the composition of the aerosol layers.

7.2.2. USE OF MARS CLIMATE SOUNDER (MCS)

MCS is a radiometer on-board Mars Reconnaissance Orbiter (MRO) that measures the radiance coming from the martian surface or atmosphere in 9 spectral bands (including the CO_2 ice absorption band). This instrument can observe at nadir but also at the limb, which enables it to sound the whole atmosphere (from 0 to 80 km altitude) [26]. Besides, its spatio-temporal coverage is a lot better than the other instruments, which enables to have more data from more points in the atmosphere. The observations at the limb help also to determine the structure of the mesospheric aerosol layers. A first study using this instrument has already been published [27]. They have very good results for the low atmosphere (from 0 to 20km altitude) but there are only 2 years of data that is not enough to characterise the high mesosphere, as the aerosol layers are constrained locally. However, they have some results about the mesospheric clouds. According to [27], the mesospheric clouds that form at Ls<150° (Northern hemisphere spring and summer) are constrained close to the equator and are majorly composed of CO_2 ice whereas the clouds that form at Ls>150° are present at midlatitudes and are majorly composed of dust and water ice. Further study with this instrument and a larger dataset are needed to conclude about the source of the condensation nuclei according to the season.

7.2.3. NEW INSTRUMENTS ON-BOARD FUTURE MISSIONS

Two instruments on-board the ExoMars Trace Gas Orbiter (TGO) may help to obtain further insight about the formation of mesospheric CO_2 clouds starting January 2018. First, ACS (Atmospheric Chemistry Suite) is an instrument composed of three spectrometers (covering a wavelength range from 0.7μm to 17μm) that will enable to do observations of the martian atmosphere at nadir and at the limb and derive vertical CO_2 profile and temperature. It will be also able to monitor clouds, dust and, more generally, the source of condensation nuclei. Second, NOMAD (Nadir and Occultation for MArs Discovery) is also a spectrometer but it will operate in two wavelength bands and cover the ultraviolet, the visible and the infrared (0.2-0.65 μm and 2.2-4.3 μm). Thanks to this instrument, il will be possible to measure the spectrum of sunlight and identify and map the martian atmosphere constituents such as the aerosols [28]. As a consequence, these instruments may be useful to characterise the CO_2 clouds.

7.2.4. NEW MODEL SCENARIOS

Section 2.2 described a martian climate model used to simulate the atmospheric processes that take place on Mars and the temperatures found with this model. Thanks to [12], the microphysics of the mesospheric clouds is understood better and soon, these will be implemented in the MGCM. With the capability of the model to describe the dust climatology as observed for different years, it will be possible to simulate the physics of the CO_2 clouds according to these dust scenarios. As a consequence, it will be possible to see of the dust lifted from the surface has a real impact on the cloud formation and if it could be a viable source for condensation nuclei. A source of condensation nuclei can also be added in the mesosphere to model the meteoritic smoke particles and test their effect on the clouds.

8 CONCLUSION

In this study, the current knowledge about the presence, the characteristics and the formation processes of mesospheric CO_2 clouds have been described and explained. The different instruments used during the thesis were also detailed and we now understand the problematic of the calibration of OMEGA and why there is less and less available data coming from this instrument. Moreover the method developed by [5] has been detailed and improved in order to sharpen the detection and avoid false detection as much as possible. Thanks to that, the study of the new orbits was easier. We have been able to establish a new list of mesospheric CO_2 clouds and analyse their main properties (Solar Longitude, Latitude, Longitude and Local Time). Besides, a newly found cloud shadow gives us the possibility to map the optical thickness and particle size pixel by pixel for this particular cloud. It also helps us to have more insight about the characteristics of the mesospheric CO_2 clouds. Finally, thanks to the Monte-Carlo code, we have been able to simulate cloud shadow observations and observe the impact of some variables (altitude, optical thickness and solar zenith angle) on the depth of the shadow.

We have seen that it is really difficult to link the clouds with atmospheric parameters such as dust as the coverage of Mars Express is not the same for every Martian Years. Another difficulty is due to the instrument aging of OMEGA. As a consequence, we cannot conclude now about the source of the condensation nuclei. We need more observations coming from other instruments to conclude about the types of particles inside a cloud and their formation process. In particular, observations at the limb are necessary to do this. By combining the results of this thesis with the ones coming from other instruments and new atmospheric models, one should be able to understand the processes that take place in the martian mesosphere and so be able to model the CO_2 clouds at the right altitude with the corresponding optical thickness and particle size as our observations. The Mars Global Climate Model (MGCM) will be then improved and it will help to reveal some characteristics of Mars that are still unknown for the moment.

A

CORRELATION WITH THE VISIBLE CHANNEL FOR CLOUDY ORBITS

Here we present some figures related to Section 5.2.1 to try to correlate the CO_2 ice absorption band with the visible channel thanks to a global study. 16 cubes have been selected: 9 contain clouds and 7 do not. The reflectance for each orbit has been plotted in Figure A.1, the red lines are for the cloudy orbits and the black for the others.

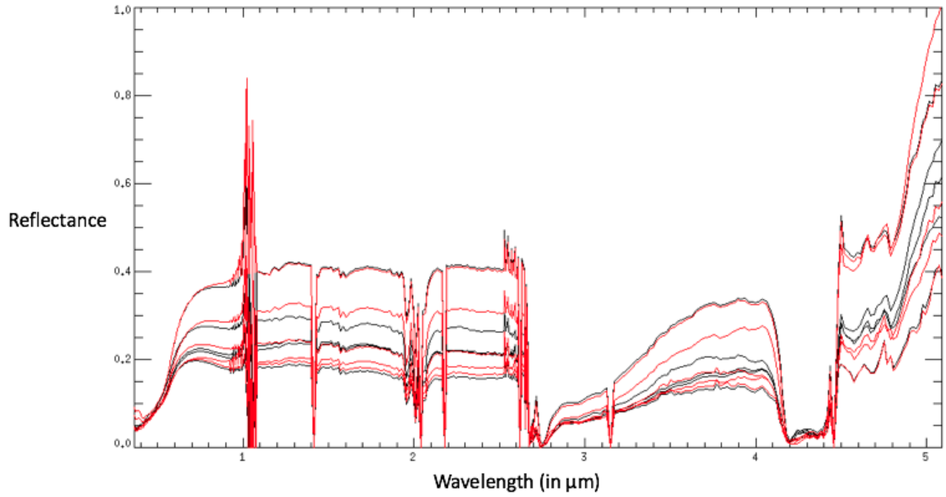

Figure A.1: Mean spectrum from 16 cubes (9 have clouds inside): the reflectances in red are for the cloudy orbits and in black the others.

It appears to be very difficult to deduce any correlations from this figure. Figure A.2 shows the same graph but only in the visible channel this time.

According to Figure A.2, there is no specific behaviour in the visible channel whether the cube contains cloud or not. The slope (between the red and the blue) is different for each orbit. The assessment of this slope has been done for several cloudy orbits (see Figure 5.4) and it is really difficult to make any conclusions.

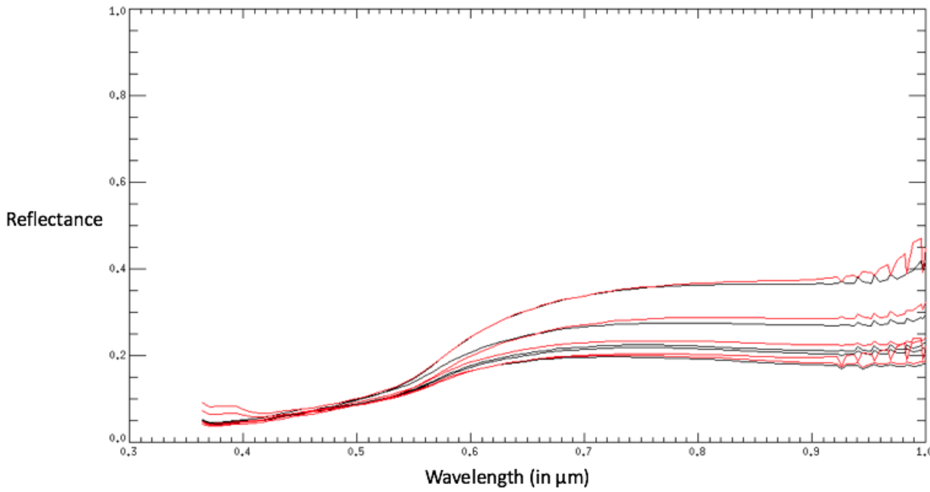

Figure A.2: Mean spectrum from 16 cubes (9 have clouds inside) in the visible channel: the reflectances in red are for the cloudy orbits and in black the others.

B

Correlation function

Here also we present some figures related to Section 5.2.1 to correlate the CO_2 ice absorption band with the visible channel thanks to the correlation function. Figures B.1, B.2 and B.3 present the correlation function for several orbits.

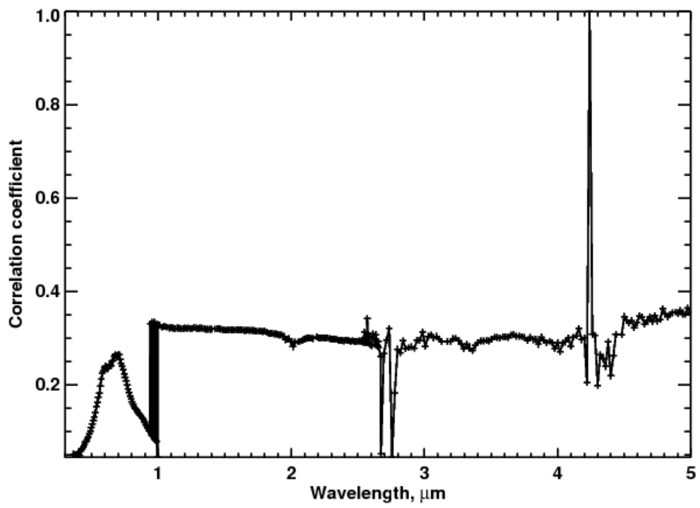

Figure B.1: Correlation function for the non-cloudy orbit #0519_1 between the 4.26μm image and the image collected at all other wavelengths.

In this case, it is also impossible to conclude anything about a correlation between the visible band and the CO_2 ice scattering peak because all the results do not depend on the existence of a cloud. They may depend on the properties of the cloud itself.

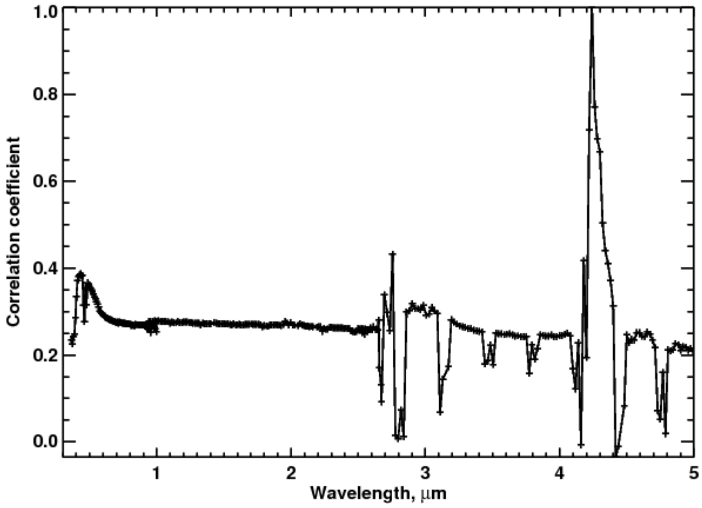

Figure B.2: Correlation function for the cloudy orbit #0551_3 between the 4.26μm image and the image collected at all other wavelengths.

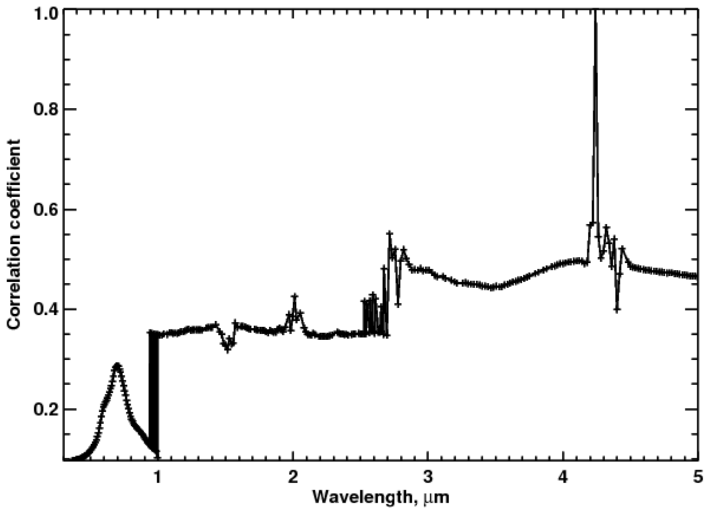

Figure B.3: Correlation function for the non-cloudy orbit #4361_4 between the 4.26μm image and the image collected at all other wavelengths.

Bibliography

[1] C. R. and S. B., *CO_2 ice clouds in the upper atmopshere of Mars,* Geophysical Research Letters **25**, 489 (1998).

[2] M. F. et al., *Subvisible CO_2 ice clouds detected in the mesosphere of Mars,* Icarus **183**, 403 (2006).

[3] M. F. et al., *Hyperspectral imaging of convective CO_2 ice clouds in the equatorial mesosphere of Mars,* Journal of Geophysical Research **112** (2007).

[4] V. M. et al., *New near-IR observations of mesospheric CO_2 and H_2O clouds on Mars,* Journal of Geophysical Research **116** (2011).

[5] M. A. et al., *Mapping the mesospheric CO_2 clouds on Mars: MEx/OMEGA and MEx/HRSC observations and challenges for atmospheric models,* Icarus **209**, 452 (2010).

[6] L. J. and de Pater I., *Fundamental Planetary Science* (Cambridge, 2013).

[7] L. C., *Modélisation des nuages de dioxyde de carbone (CO_2) sur Mars: application aux nuages mésosphériques*, Ph.D. thesis, Université Pierre et Marie Curie (2013).

[8] G.-G. F. M. A. F. F., and S. A., *The martian mesosphere revealed by CO_2 cloud observations and General Circulation Modeling,* Icarus **216**, 10 (2011).

[9] M. A. P. K. M. F., and H. A., *Mesospheric clouds on Mars and on Earth,* Comparative Climatology of Terrestrial Planets , 393 (2013).

[10] S. A. et al., *Gravity waves, cold pockets and CO_2 clouds in the Martian mesosphere,* Geophysical Research Letters **39** (2012).

[11] L. J., *Phase equilibrium in the system co_2-h_2o: Application to mars,* Journal of Geophysical Research **111** (2006).

[12] L. C. M. A. M. F. S. A., and L. F., *Modeling the microphysics of CO_2 ice clouds within wave-induced cold pockets in the martian mesosphere,* Icarus **237**, 239 (2014).

[13] L. C. M. A. R. I. M. F. and L. F., *Near-pure vapor condensation in the martian atmosphere: CO_2 ice crystal growth,* Journal of Geophysical Research **118**, 1 (2013).

[14] C. R. et al., *Mars equatorial mesospheric clouds: Global occurence and physical properties from Mars Global Surveyor Thermal Emission Spectrometer and Mars Orbiter Camera limb observations,* Journal of Geophysical Research **112** (2007).

[15] S. F. et al., *Concatenation of HRSC colour and OMEGA data for the determination and 3D-parameterization of high-altitude CO_2 clouds in the Martian atmosphere,* Planetary and Space Science (2010).

[16] M. T. et al., *THEMIS-VIS observations of clouds in the martian mesosphere: Altitudes, wind speeds, and decameter-scale morphology,* Icarus **210**, 545 (2010).

[17] B. J.-P. et al., *Omega : Observatoire pour la minéralogie, l'eau, les glaces et l'activité,* ESA SP **1240**, 37 (2004).

[18] B. J.-P. et al., *Mars surface diversity as revealed by the omega/mars express observation,* Science **307**, 1576 (2005).

[19] B. G. et al., *The ground calibration setup of omega and virtis experiments: Description and performances,* Planetary and Space Science **53**, 711 (2005).

[20] J. D. et al., *OMEGA long wavelength channel: Data reduction during non-nominal stages,* Planetary and Space Science **57**, 1032 (2009).

[21] A. J. et al., *Mars surface thermal inertia and heterogeneities from OMEGA/MEX,* Icarus **233**, 194 (2014).

[22] J. R. et al., *The high-resolution stereo camera (HRSC) experiment on Mars Express: Instrument aspects and experiment conduct from interplanetary cruise through the nominal mission,* Planetary and Space Science **55**, 928 (2007).

[23] B. J. et al., *SPICAM on Mars Express: Observing modes and overview of UV spectrometer data and scientific results,* Journal of Geophysical Research **111** (2006).

[24] S. M. D., *Spacecraft observations of the martian atmosphere,* Annual Review of Earth and Planetary Sciences **36**, 191 (2008).

[25] H. M. et al., *The content and composition of meteroic smoke in mesospheric ice particles from sofie observations,* Journal of Atmospheric and Solar-Terrestrial Physics **84-85**, 1 (2012).

[26] M. D. et al., *Mars climate sounder: An investigation of thermal and water vapour structure, dust and condensate distributions in the atmosphere, and energy balance of the polar regions,* Journal of Geophysical Research **112**, 1 (2007).

[27] S.-N. E. et al., *Climatology and first-order composition estimates of mesospheric clouds from mars climate sounder limb spectra,* Icarus **222**, 342 (2013).

[28] V. A. et al., *Science objectives and performances of nomad, a spectrometer suite for the exomars tgo mission,* Planetary and Space Science **119**, 233 (2015).